Boosting photothermal conversion through simultaneous donor engineering for solar driven applications

Yitian Pan [a], Derong Cao [a], Xueguang Ran [b], Lingyun Wang [*,a]

Supplementary Information

1. Reagents and materials

All solvents and reagents are purchased from Energy Chemical and Bidepharm for direct use. ^{1}H NMR spectrum was measured on a Bruker ARX 400 MHz. Mass Spectrum was measured on MALDI-TOF-MS. Thermogravimetric analysis (TGA) was performed on a TA Q500 thermogravimeter by measuring their weight loss while heating at a rate of 10 K min^{-1} from 20 to 600 °C under nitrogen. The solar-driven water evaporation experiments were conducted on Solar simulator with an optical filter for the standard AM 1.5 G spectrum (CEL-S500/350/150). In this experiment, the irradiation intensity is one solar irradiation intensity (1.0 kW m^{-2}). The surface temperature of the foam was recorded by an IR thermal camera (FLIR E4). The weight loss of water was measured by an electronic mass analytical balance (Sartorius BSA224S). The ion concentration in seawater was measured by Inductively Coupled Plasma Spectroscopy (ICP-OES, Agilent 5110). The Photothermal Property of powder samples were obtained on 808 nm Fiber Coupled Laser (Model: MW-GX-808, Changchun Laser Optoelectronics Technology Co., Ltd.) and the surface temperature of the powder was recorded by the IR thermal camera (FLIR E4).

2. Methods

2.1 Synthesis

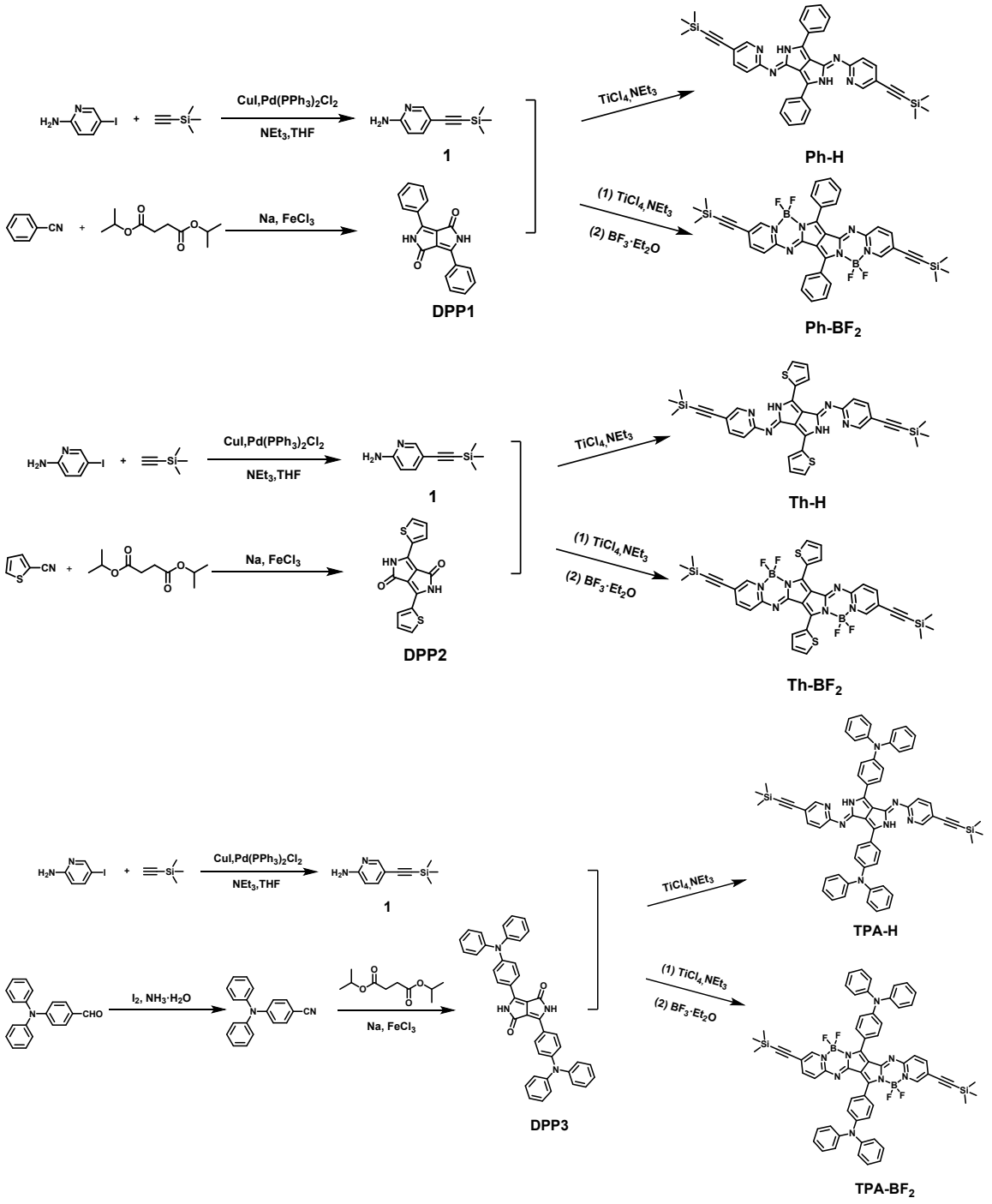

Compounds **1**, **DPP1**, **DPP2**, and **DPP3** were synthesized according to our previous literatures [14, 15].

Synthesis of Ph-H: Under nitrogen atmosphere, **1** (800 mg, 4.2 mmol) and **DPP1** (200 mg, 0.69 mmol) were added to a dry toluene (15 mL). After heating to 110 °C, titanium tetrachloride (0.5 mL, 4.83 mmol) and triethylamine (2.6 mL, 18.6 mmol) were successively added and stirred for 3 h. After removing the solvents, the residue was

purified by column chromatography (hexane/dichloromethane = 2:1) to give the crude solid. Then, crude compound was further purified by precipitation with dichloromethane / methanol to afford **Ph-H** as a blue solid (234 mg) in yield of 53%. ^{1}H NMR (400 MHz, $CDCl_3$): δ 13.10 (s, 2H), 8.47 (m, 6H), 7.72 (d, *J* = 8.4 Hz, 2H), 7.53 (m, 6H), 7.34 (d, *J* = 8.4 Hz, 2H), 0.25 (s, 18H). MALDI-TOF (%): Calcd. For $[M+Na+H]^{2+}$ $C_{38}H_{37}N_6Si_2Na$, m/z: 656.2505; found, 656.0787.

Synthesis of Ph-BF_2: Under nitrogen atmosphere, **1** (800 mg, 4.2 mmol) and **DPP1** (200 mg, 0.69 mmol) were added to a dry toluene (15 mL). After heating to 110 ^{o}C, titanium tetrachloride (0.5 mL, 4.83 mmol) and triethylamine (2.6 mL, 18.6 mmol) were successively added and stirred for 3 h. The consumption of **DPP1** was monitored by TLC. Then, borontrifluoride etherate (1.0 mL, 8.64 mmol) was added and refluxed for another 4 h. Upon cooling to room temperature, the reaction mixture was poured into water and extracted with dichloromethane. The crude compound was purified by silica gel column chromatography (hexane/dichloromethane = 3:1) to afford **Ph-BF_2** as a blue solid (213 mg) in yield of 42%. ^{1}H NMR (400 MHz, $CDCl_3$): δ 8.35 (m, 6H), 7.78 (d, *J* = 6.8 Hz, 2H), 7.56 (m, 6H), 7.18 (d, *J* = 7.2 Hz, 2H), 0.25 (s, 18H). MALDI-TOF (%): Calcd. For $[M+Na+H]^{2+}$ $C_{38}H_{35}B_2F_4N_6Si_2Na$, m/z: 752.2482; found, 752.1837.

Synthesis of Th-H: The synthetic method is similar to the synthesis of **Ph-H**, Under nitrogen atmosphere, **1** (365 mg, 1.92 mmol) and **DPP2** (100 mg, 0.32 mmol) were added to a dry toluene (10 mL). After heating to 110 ^{o}C, titanium tetrachloride (0.25 mL, 2.24 mmol) and triethylamine (1.2 mL, 8.64 mmol) were successively added and stirred for 3 h. After removing the solvents, the residue was purified by column chromatography (hexane/dichloromethane = 2:1) to give the crude solid. Then, crude compound was further purified by precipitation with dichloromethane / methanol to generate **Th-H** as a dark blue solid (86 mg) in yield of 42%. ^{1}H NMR (400 MHz, $CDCl_3$): δ 12.72 (s, 2H), 8.76 (s, 2H), 8.48 (s, 2H), 7.69 (d, *J* = 8.4 Hz, 2H), 7.56 (s, 2H), 7.33 (m, 2H), 7.23 (m, 2H), 0.29 (s, 18H). MALDI-TOF (%): Calcd. For $[M+Na+H]^{2+}$ $C_{34}H_{33}N_6S_2Si_2Na$, m/z: 668.1644; found, 668.0009.

Synthesis of Th-BF_2: The synthetic method is similar to the synthesis of **Ph-BF_2**,

Under nitrogen atmosphere, **1** (1.46 g, 7.68 mmol) and **DPP2** (400 mg, 1.28 mmol) were added to a dry toluene (30 mL). After heating to 110 °C, titanium tetrachloride (1.0 mL, 8.96 mmol) and triethylamine (4.8 mL, 34.56 mmol) were successively added and stirred for 3 h. The consumption of **DPP2** was monitored by TLC. Then, borontrifluoride etherate (3.9 mL, 30.72 mmol) was added and refluxed for another 5 h. Upon cooling to room temperature, the reaction mixture was poured into water and extracted with dichloromethane. The crude compound was purified by silica gel column chromatography (hexane/dichloromethane = 3:1) to afford **Th-BF_2** as a green solid (445 mg) in yield of 47%. ^{1}H NMR (400 MHz, $CDCl_3$): δ 9.11 (s, 2H), 8.41 (s, 2H), 7.78 (m, 4H), 7.32 (d, *J* = 7.2 Hz, 2H), 7.28 (m, 2H), 0.28 (s, 18H). MALDI-TOF (%): Calcd. For $[M+Na+H]^{2+}$ $C_{34}H_{31}B_2F_4N_6S_2Si_2Na$, m/z: 764.1610; found, 764.1060.

Synthesis of TPA-H: The synthetic method is similar to the synthesis of **Ph-H**, Under nitrogen atmosphere, **1** (365 mg, 1.92 mmol) and **DPP3** (200 mg, 0.32 mmol) were added to a dry toluene (18 mL). After heating to 110 °C, titanium tetrachloride (0.25 mL, 2.24 mmol) and triethylamine (1.2 mL, 8.64 mmol) were successively added and stirred for 2 h. After removing the solvents, the residue was purified by column chromatography (hexane/dichloromethane = 1:1) to give the crude solid. Then, crude compound was further purified by precipitation with dichloromethane / methanol to generate **TPA-H** as a green solid (105 mg) in yield of 34%. ^{1}H NMR (400 MHz, $CDCl_3$): δ 13.01 (s, 2H), 8.43 (m, 4H), 7.62 (d, *J* = 8.4 Hz, 2H), 7.34 (t, J = 8.0 Hz, 10H), 7.20 (d, *J* = 8.0 Hz, 10H), 7.15 (t, *J* = 7.2 Hz, 8H), 0.25 (s, 18H). MALDI-TOF (%): Calcd. for $[M+H]^+$ $C_{62}H_{55}N_8Si_2$, m/z: 967.4083; found, 967.2714.

Synthesis of TPA-BF_2: The synthetic method is similar to the synthesis of **Ph-BF_2**, Under nitrogen atmosphere, **1** (365 mg, 1.92 mmol) and **DPP3** (200 mg, 0.32 mmol) were added to a dry toluene (20 mL). After heating to 110 °C, titanium tetrachloride (0.25 mL, 2.24 mmol) and triethylamine (1.2 mL, 8.64 mmol) were successively added and stirred for 2 h. The consumption of **DPP3** was monitored by TLC. Then, borontrifluoride etherate (3.9 mL, 30.72 mmol) was added and refluxed for another 4 h. Upon cooling to room temperature, the reaction mixture was poured into water and extracted with dichloromethane. The crude compound was purified by silica gel column

chromatography (hexane/dichloromethane = 2:1) to afford **TPA-BF_2** as a dark violet solid (44 mg) in yield of 13%. ^{1}H NMR (400 MHz, $CDCl_3$): δ 8.42 (d, *J* = 8.7 Hz, 4H), 8.31 (d, *J* = 2.1 Hz, 2H), 7.71 (dd, J_1 = 8.9 Hz, J_2= 2.1 Hz, 2H), 7.35 (t, *J* = 7.7 Hz, 8H), 7.27-7.25 (m, 4H), 7.25 (d, *J* = 6.2 Hz, 4H), 7.16 (t, *J* = 7.3 Hz, 6H), 7.10 (d, J = 8.7 Hz, 4H), 0.25 (s, 18H). MALDI-TOF (%): Calcd. for $[M+H]^+$ $C_{62}H_{53}B_2F_4N_8Si_2$, m/z: 1063.4048; found, 1063.0260.

2.2 Theoretical Calculation

All simulations were implemented for isolated molecules using the Gaussian 16 software package (ref Gaussian 16 Rev. B.01, 2016.). The calculations are performed using density generalized function theory (DFT) and time-dependent DFT (TD-DFT) methods. The geometric optimization was using DFT at the high-nonlocality hybrid functional M06-2X (ref 10.1007/s00214-007-0310-x) with the 6-311G (d,p) basis set. In all the cases, frequency analysis was made after geometry optimization to ensure the convergence to an energy minimum. TD-DFT calculations were done at S_0 optimized geometries using M06-2X /6-311G (d,p).

2. 3 Measurement of absolute photoluminescence quantum yield (PLQY)

Fluorescence quantum yields is a key parameter for evaluating the molecular luminescence efficiency. The absolute photoluminescence quantum yield (PLQY) of six molecules in chloroform was measured with a Hamamatsu C11347 instrument by integrating sphere method.

Sample	Excitation (nm)	Absorbance	Transmittance	Quantum efficiency	Number of photons (Abs)	Number of photons (Ex)	Number of photons (FL)
Ph-H	630	0.917	0.083	0.028	6.054e+10	6.605e+10	1.846e+9
Ph-BF_2	630	0.889	0.111	0.478	5.873e+10	6.605e+10	3.158e+10
Th-H	630	0.749	0.251	0.032	4.944e+10	6.605e+10	2.134e+9
Th-BF_2	630	0.991	0.009	0.175	6.543e+10	6.605e+10	1.158e+10
TPA-H	630	0.921	0.079	0.133	6.083e+10	6.605e+10	8.830e+9
TPA-BF_2	690	0.845	0.155	0.011	4.950e+10	5.855e+10	6.621e+8

2.4 Preparation of photothermal material-loaded sponge

A commercially available polyurethane sponge (2 cm radius) was utilized as a carrier. 5 mg powder was dissolved in CH_2Cl_2 (5 mL). The powder-loaded PU foam was obtained by soaking into CH_2Cl_2 solution. Then, the wet PU was placed in an oven for 3 hours under 60 °C.

2.5 Water evaporation experiment

In the environment of 24-25 °C and 30-40 % relative humidity, the water-filled beaker with sponge is placed on the analytical balance. Under the irradiated of simulated sunlight with an intensity of 1 kW m^{-2} (one sun), we recorded the balance reading every five minutes (representing the lost water mass). After one hour, the twelve data points can be used to fit the water evaporation curves. For the seawater desalination experiment, the water was replaced with seawater under the same conditions.

2.6 Calculation of photothermal conversion efficiency (PCE)

The 1 mg sample power was dispersed in 1 mL water in a container with an insulating layer and the solution was illuminated with simulated solar light. The container is a white polypropylene lid with a diameter of 1.5 cm and Figure 4o records the final temperature reached by the sample under simulated solar irradiation, with an identical pure water sample serving as the blank control. The temperature of the solution was recorded using an infrared thermal imager upon simulated solar light irradiation for 15 minutes and energy conversion efficiency (η) was calculated as the following formula:

$$\eta = \frac{Q}{E} = \frac{Q_1 - Q_2}{E}$$

Where Q refers to the thermal energy generated (i.e., $Q = Q_1 - Q_2$), Q_1 is the thermal energy generated of the photothermal material sample and Q_2 is the thermal energy generated of pure water. E refers to the total energy of the incident light. Q is determined by the heat capacity (C), density (ρ), volume (V) and ΔT over the period of irradiation of the solution; E is determined by the power (P) of the incident light, the irradiation

area (S) and irradiation time (t). Therefore, the specific formula is as follows:

$Q_1 = C\rho V\Delta T_1$

$Q_2 = C\rho V\Delta T_2$

$E = PSt$

In this paper, since samples are present in very low amounts in the solution, values of C (4.2 J g^{-1} °C $^{-1}$) and ρ (1 g cm^{-3}) for water were used in the calculations.

For example, the surface temperature of TPA-BF_2 dispersion was 46.5 °C during the irradiation process, and the initial temperature is 25.0 °C, therefore ΔT_1 is 21.5 °C. As the control, the temperature of pure water raised from 25.0 °C to 36.5 °C, so ΔT_2 is 11.5 °C.

As the above formulas:

$Q_1 = C\rho V\Delta T_1 = 4.2 \times 1 \times 1 \times (46.5 - 25.0) = 90.3$ J

$Q_2 = C\rho V\Delta T_2 = 4.2 \times 1 \times 1 \times (36.5 - 25.0) = 48.3$ J

$E = P\ S\ t = 1000 \times 3.14 \times (1.5 / 2 \times 10^{-2})^2 \times 900 = 158.96$ J

$\eta = (Q_1 - Q_2) / E = (90.3 - 48.3) / 158.96 = 26.4\%$

As a result, the PCE of TPA-BF_2 was 26.4%.

The surface temperature of six molecules was shown in a Table. Based on the same method, the PCE of Ph-H, Ph-BF_2, Th-H, Th-BF_2 and TPA-H were calculated to be 9.8%, 8.4%, 14.0%, 22.0% and 18.0%.

Compound	Initial temperature(°C)	Final temperature(°C)	ΔT_1 (°C)	PCE (%)
Ph-H	25.0	40.2	15.2	9.8
Ph-BF_2	25.0	39.7	14.7	8.4
Th-H	25.0	41.8	16.8	14.0
Th-BF_2	25.0	44.8	19.8	22.0
TPA-H	25.0	43.3	18.3	18.0
TPA-BF_2	25.0	46.5	21.5	26.4
Pure water	25.0	36.5	11.5	-

2.7 Calculation of the efficiency for solar to vapor generation:

efficiency η of solar energy in photothermal assisted water evaporation was calculated as the following formula:

$$\eta = \frac{\dot{m} h_{LV}}{C_{opt} P_0}$$

Where $\dot{m}$ refers to the mass flux (evaporation rate) of water, h_{LV} refers to the total liquid vapor phase-change enthalpy (i.e., the sensible heat and the enthalpy of vaporization (i.e., $h_{LV} = Q + \Delta h_{vap}$)), Q is the energy provided to heat the system from the initial temperature to a final temperature , Δh_{vap} is the latent heat of vaporization of water, P_0 is the nominal solar irradiation value of 1 kW m^{-2}, and C_{opt} represents the optical concentration. The schematic for the vaporization enthalpy of the vapor is displayed as follows.

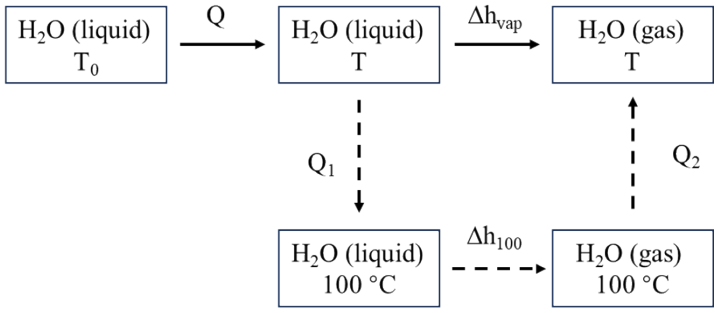

$$Q = C_{liquid}(T - T_0)$$

$$\Delta h_{vap} = Q_1 + \Delta h_{100} + Q_2$$

$$Q_1 = C_{liquid}(100 - T)$$

$$Q_2 = C_{vapor}(T - 100)$$

In this paper, C_{liquid}, the specific heat capacity of liquid water is a constant of 4.18 J (g °C) $^{-1}$, C_{vapor}, the specific heat capacity of water vaper is a constant of 1.865 J (g °C) $^{-1}$, Δh_{100} is the latent heat of vaporization of water at 100 °C, taken to be 2260 kJ kg^{-1}.

2.8 Calculation of the energy efficiency

Sunlight is absorbed by photothermal materials and converted into heat energy. In addition to the heat energy used for water evaporation at the interface, thermal radiation loses part of the heat energy to the surrounding environment. In addition, loss of heat convection with nearby fluids, and loss of heat conduction to bulk phase water will also

happen. According to the above energy input and loss links, we can get the following equation to express the relationship between incident light power P_0 and evaporation power P_{evap}:

$P_0 = P_{evap} + P_{ref} + P_{rad} + P_{conv} + P_{cond}$ (1)

where P_{ref} is the light power reflected by the material, which depends on the material's properties and the incident light. P_{rad} is the power lost by heat radiation, which is affected by materials and the surrounding environment. P_{conv} is the power lost by heat convection, which is determined by the material and surrounding fluid. P_{cond} is the power loss of heat conduction to bulk water, which is affected by the material function, system structure, and water temperature. To increase P_{evap} as much as possible, researchers have spent much effort to reduce ($P_{evap} + P_{ref} + P_{rad} + P_{conv} + P_{cond}$). Heat transfer is divided into heat radiation, heat convection, and heat conduction.

According to literature, we perform the calculation of energy efficiency in the case of water evaporation as follows (taking **TPA-BF$_2$** as an example).

(1) Calculation of conduction loss η_{cond}

The conductive heat flux from **TPA-BF$_2$** + PU to water is calculated as follow:

$$P_{cond} = \frac{Cm\Delta T}{At} = \frac{4.18 \times 10 \times 1.6}{3.14 \times 10^{-4} \times 3600} = 59.2\ W\ m^{-2}$$

$$\eta_{cond} = \frac{P_{cond}}{P_{in}} = \frac{59.2}{1000} = 5.92\%$$

Where C is the specific heat capacity of liquid water (4.18 J/g ℃), t is the irradiation time (3600 s), m is the water weights (~ 10 g) and ΔT is increased temperature of the bulk water within 30 min, A is the projected area ($3.14 \lozenge 10^{-4}$ m^2).

(2) Calculation of radiation loss η_{rad}:

The radiation flux is based on Stefan-Boltzmann law, which is calculated as follow:

$$P_{rad} = \varepsilon\sigma\left(T_2^4 - T_1^4\right) = 0.85 \times 5.67 \times 10^{-8} \times \left(316.25^4 - 298.15^4\right)$$

$$= 101.2\ W\ m^{-2}$$

$$\eta_{rad} = \frac{P_{rad}}{P_{in}} = \frac{101.2}{1000} = 10.12\%$$

where ε (0.85) is the emissivity (the emissivity should be calculated using an absorption spectrum and plank formula but given that our TPA-BF_2/PU composite appears dark and has a porous structure conducive to light trapping, we adopt an emissivity value of ε = 0.85 for the heat loss calculation), σ is the Stefan–Boltzmann constant 5.67×10^{-8} W $(m^2 K^4)^{-1}$, T_2 (316.25 K) is the temperature at the surface of **TPA-BF_2** + PU steam generator, T_1 (298.15 K) is the temperature of the adjacent environment of steam generator.

(3) Calculation of convection loss η_{conv}:

$$P_{conv} = h(T_2 - T_1) = 5 \times (316.25 - 298.15) = 90.5\ W\ cm^{-2}$$

$$\eta_{conv} = \frac{P_{conv}}{P_{in}} = \frac{90.5}{1000} = 9.05\%$$

Where h is the heat transfer coefficient is approximately 5 W /m^2 K according to the previously reports. T_2 (316.25 K) is the temperature at the surface of **TPA-BF_2** + PU, T_1 (298.15 K) is the temperature of the adjacent environment of steam generator.

Lost sunlight energy: 5.92%+10.12%+9.05%=25.09%

For **TPA-BF_2**, 25.09% of the energy is wasted and 74.46% of the energy being utilized. The corresponding data for **Ph-H**, **Ph-BF_2**, **Th-H**, **Th-BF_2** and **TPA-H** were calculated with the similar method (Table S2).

Summary of heat loss of four materials.

	η_{cond}	η_{rad}	η_{conv}	$\eta_{utilized}$
TPA-BF_2	5.92%	10.12%	9.05%	74.91%
TPA-H	5.55%	9.58%	8.6%	76.27%
Th-BF_2	6.29%	9.88%	8.8%	75.03%
Th-H	5.36%	9.01%	8.2%	77.43%
Ph-BF_2	4.81%	7.61%	6.95%	80.63%
Ph-H	5.18%	8.92%	8.05%	77.85%

3. Supplementary figures and tables

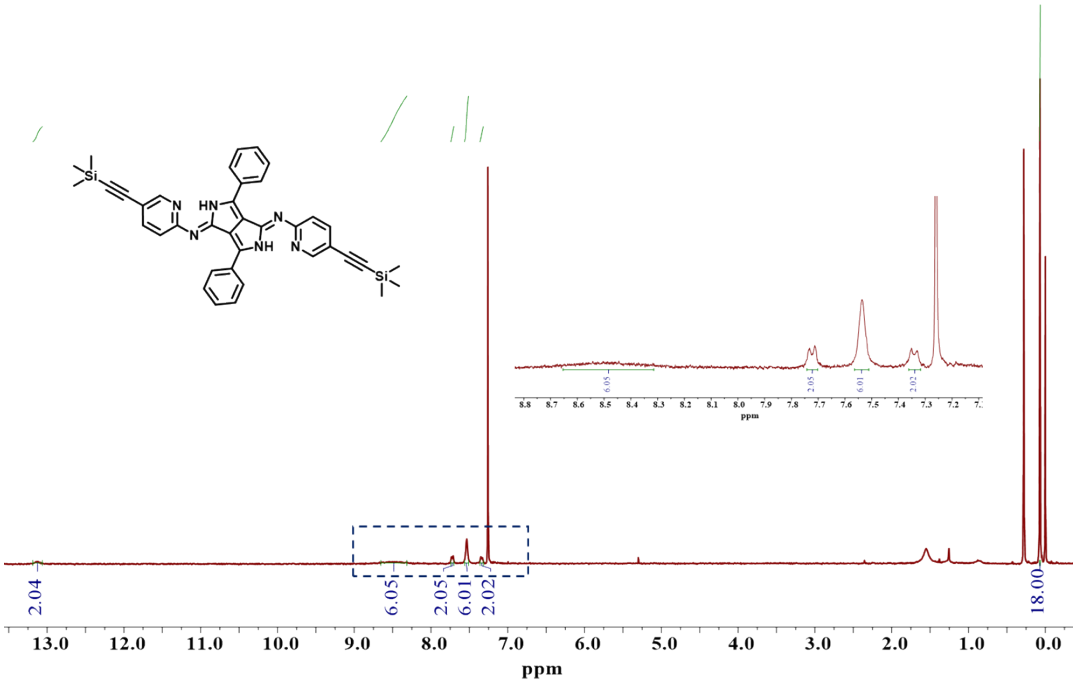

Figure S1. ^{1}H NMR (400MHz, $CDCl_3$) spectrum of compound **Ph-H.**

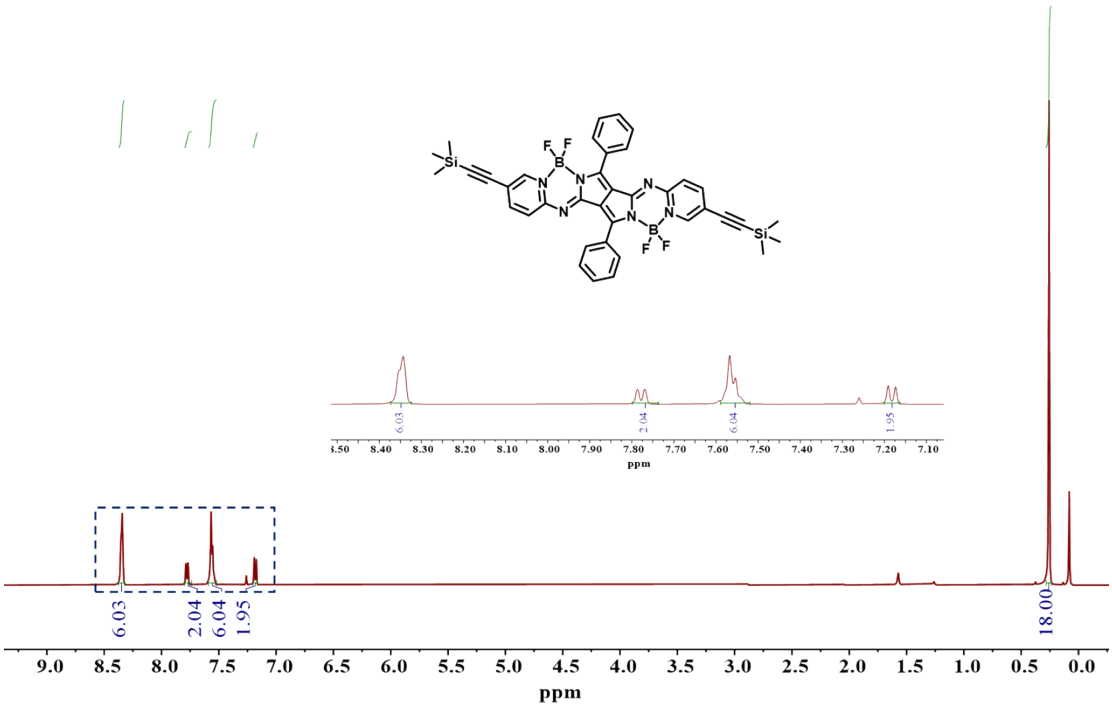

Figure S2. ^{1}H NMR (400MHz, $CDCl_3$) spectrum of compound **Ph-BF_2.**

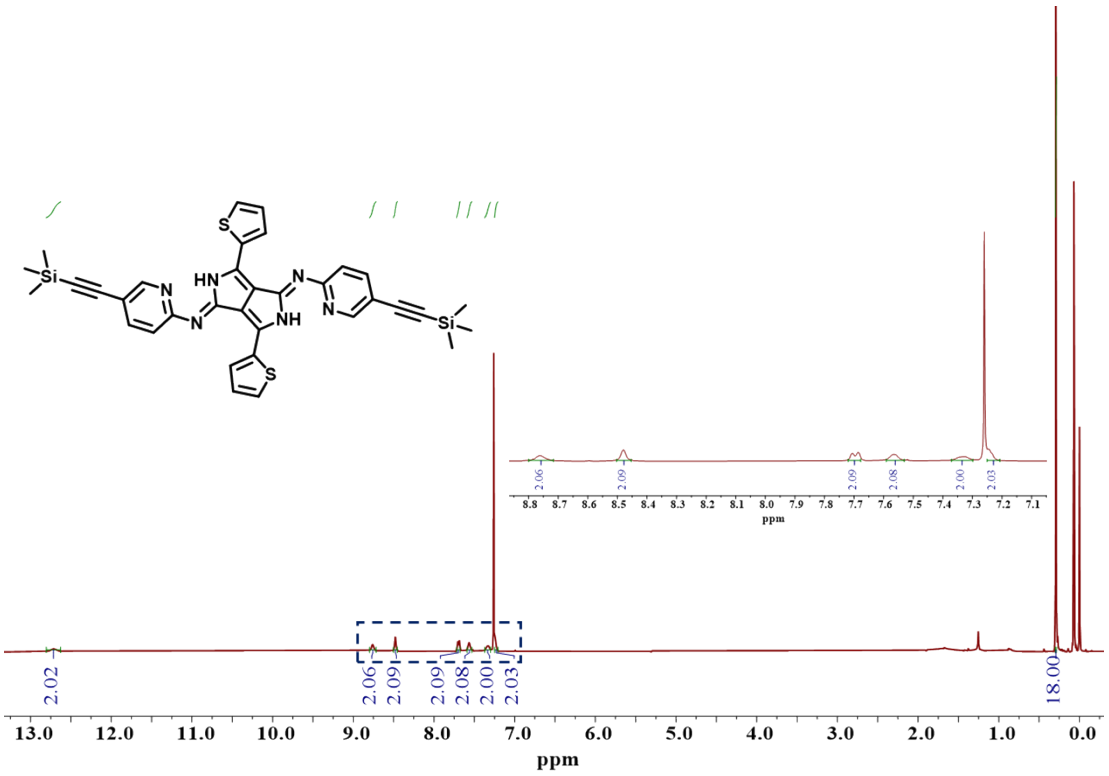

Figure S3. ^{1}H NMR (400MHz, $CDCl_3$) spectrum of compound **Th-H.**

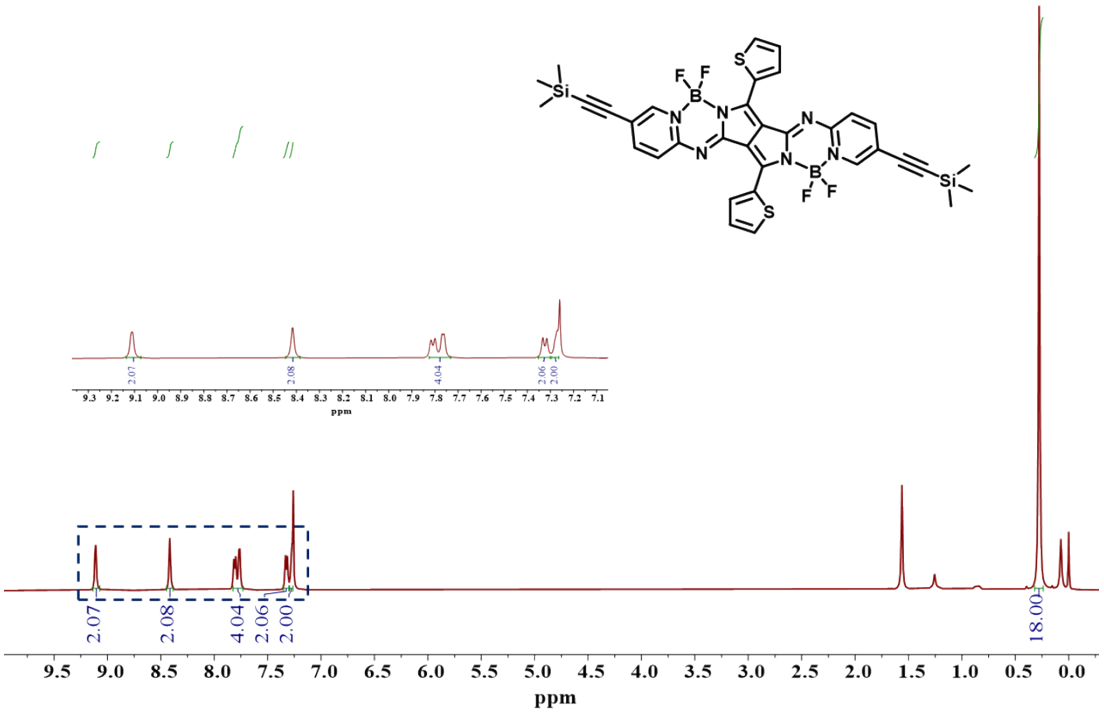

Figure S4. ^{1}H NMR (400MHz, $CDCl_3$) spectrum of compound **Th-BF_2.**

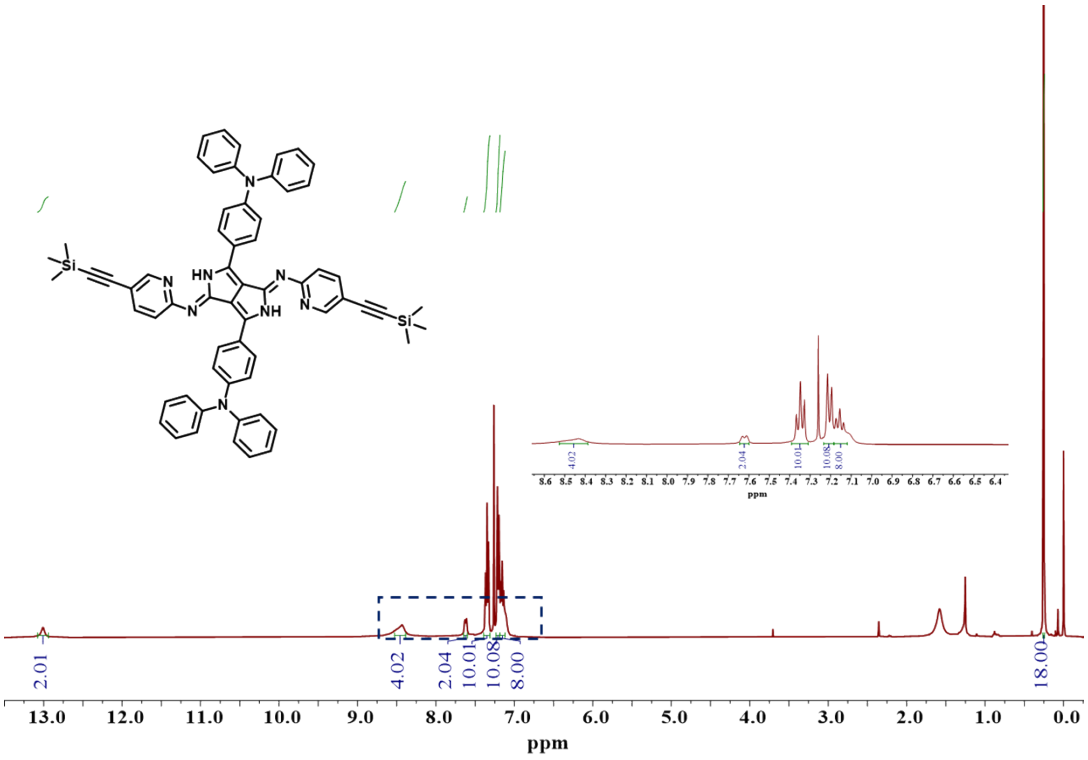

Figure S5. ^{1}H NMR (400MHz, $CDCl_3$) spectrum of compound **TPA-H.**

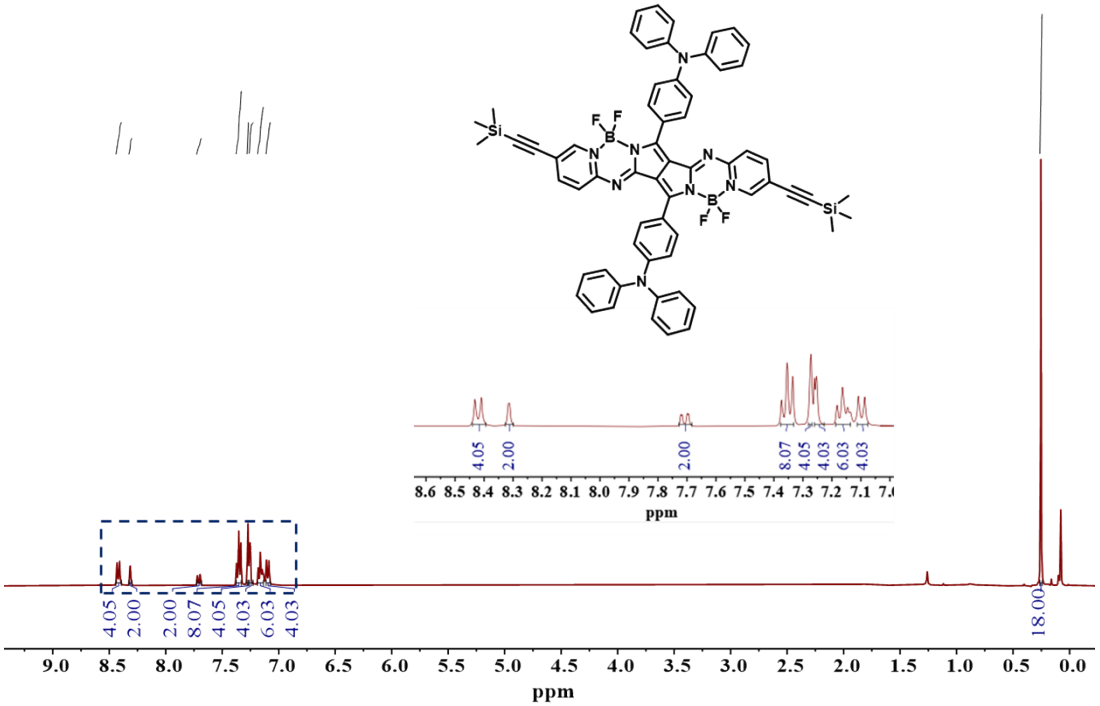

Figure S6. ^{1}H NMR (400MHz, $CDCl_3$) spectrum of compound **TPA-BF_2.**

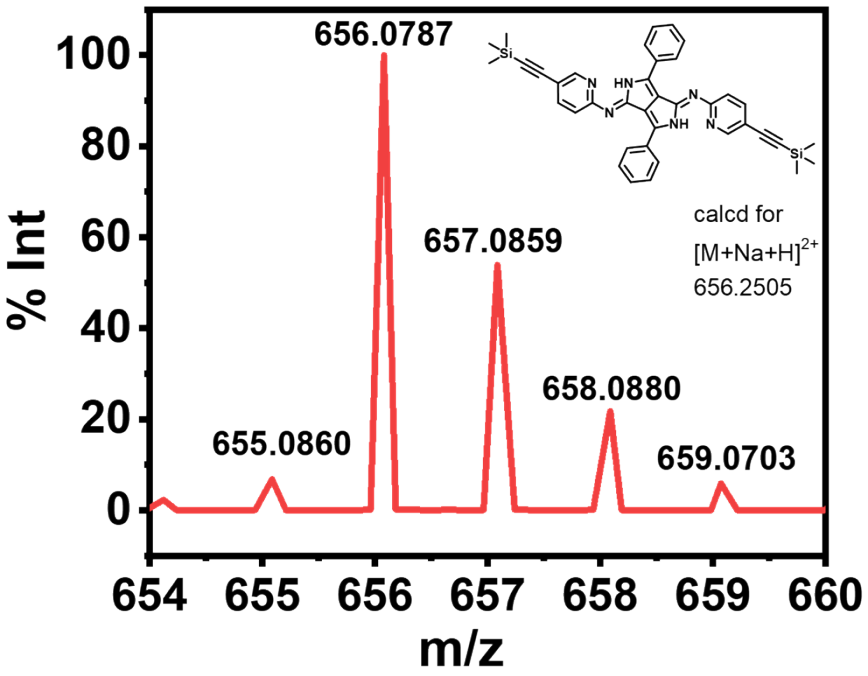

Figure S7. MALDI-TOF-MS of **Ph-H.**

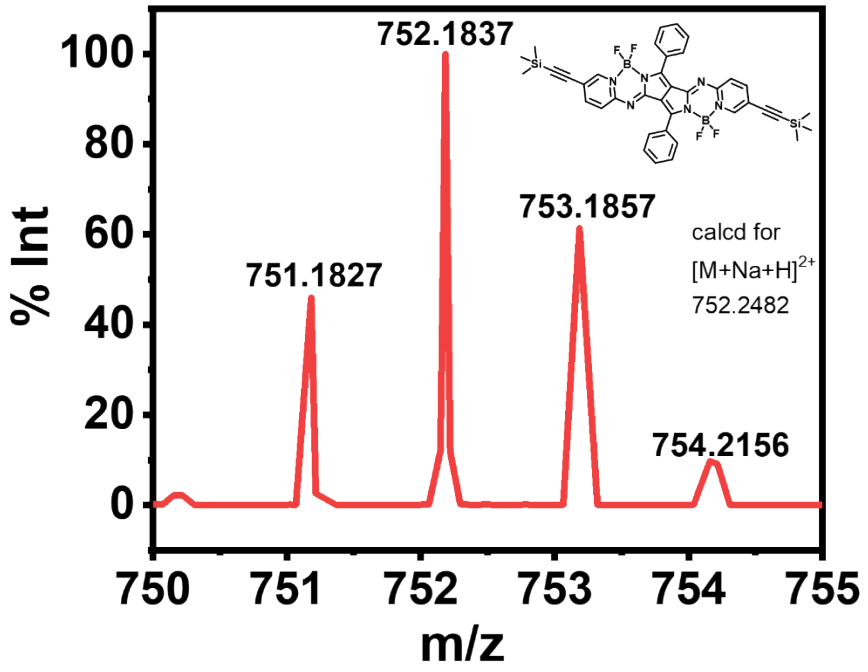

Figure S8. MALDI-TOF-MS of **Ph-BF_2.**

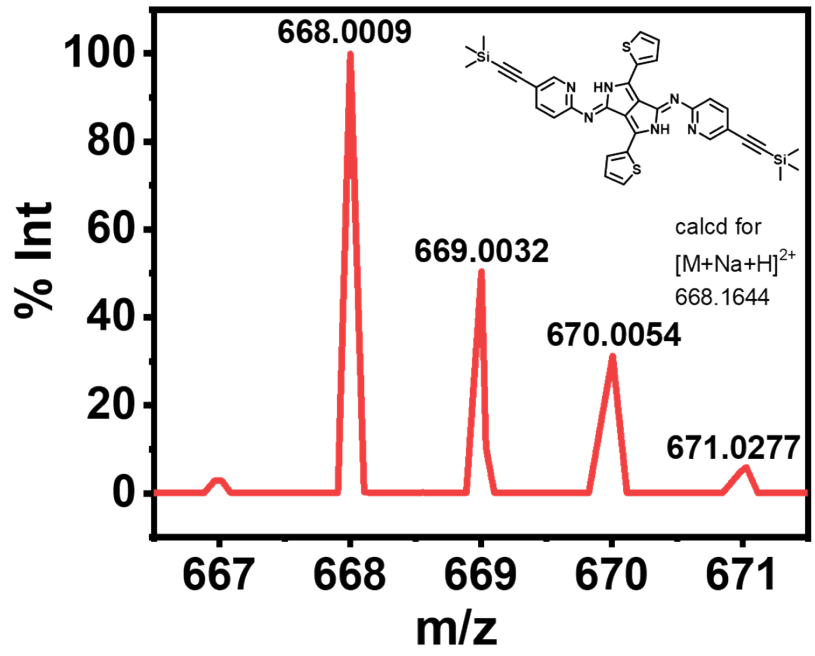

Figure S9. MALDI-TOF-MS of **Th-H.**

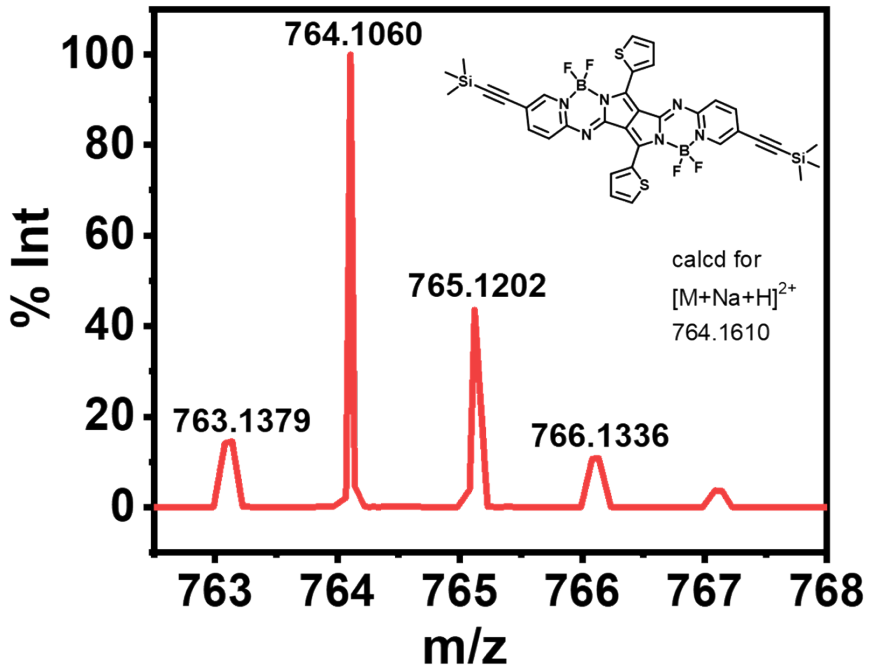

Figure S10. MALDI-TOF-MS of **Th-BF_2.**

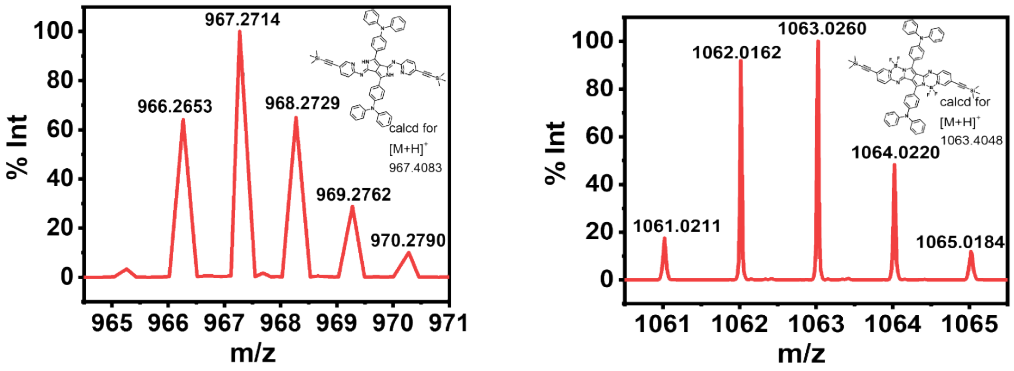

Figure S11. MALDI-TOF-MS of (left) **TPA-H** and (right) **TPA-BF$_2$.**

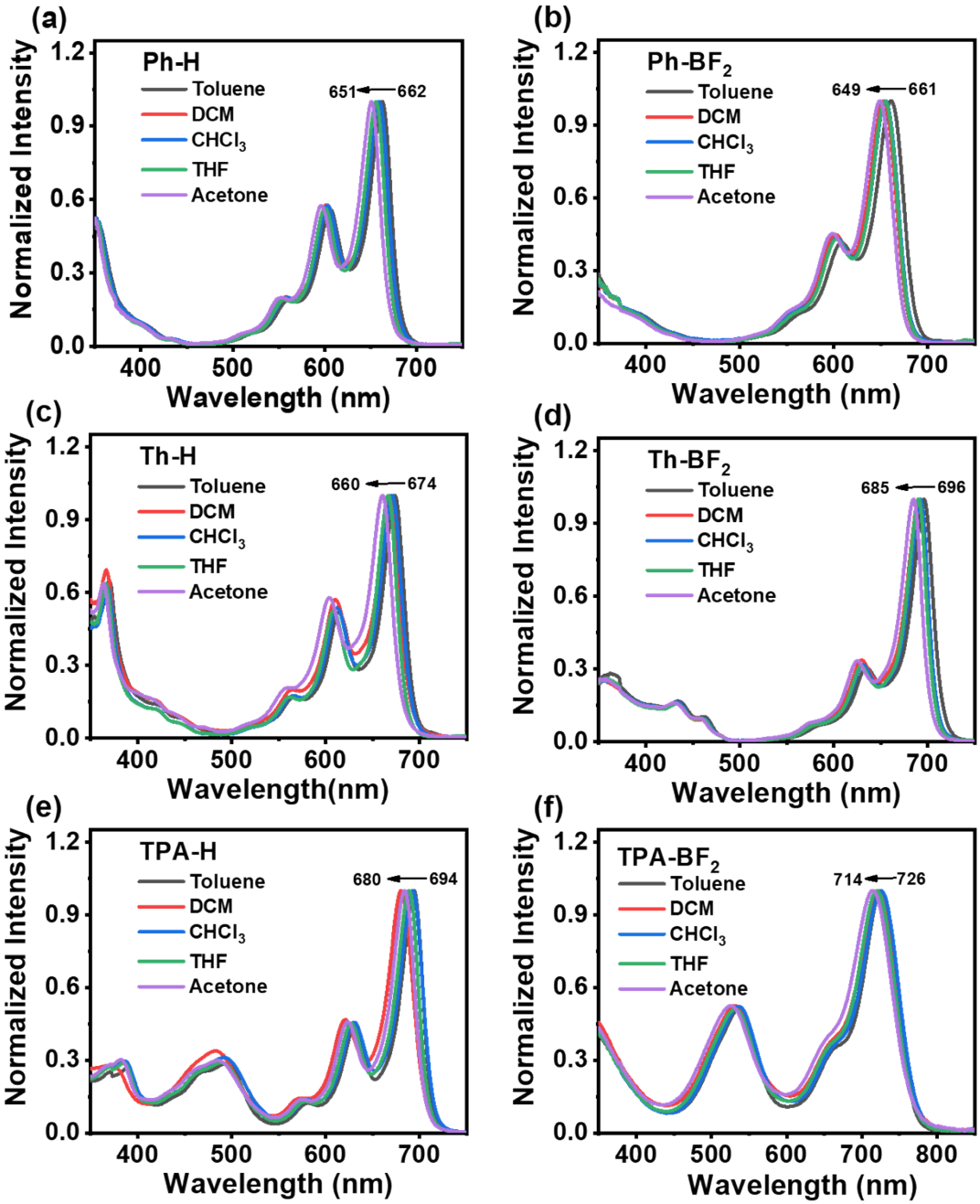

Figure S12. The UV-vis-NIR absorption spectra of (a) **Ph-H,** (b) **Ph-BF$_2$,** (c) **Th-H,** (d) **Th-BF$_2$,** (e) **TPA-H** and (f) **TPA-BF$_2$** in different solvents.

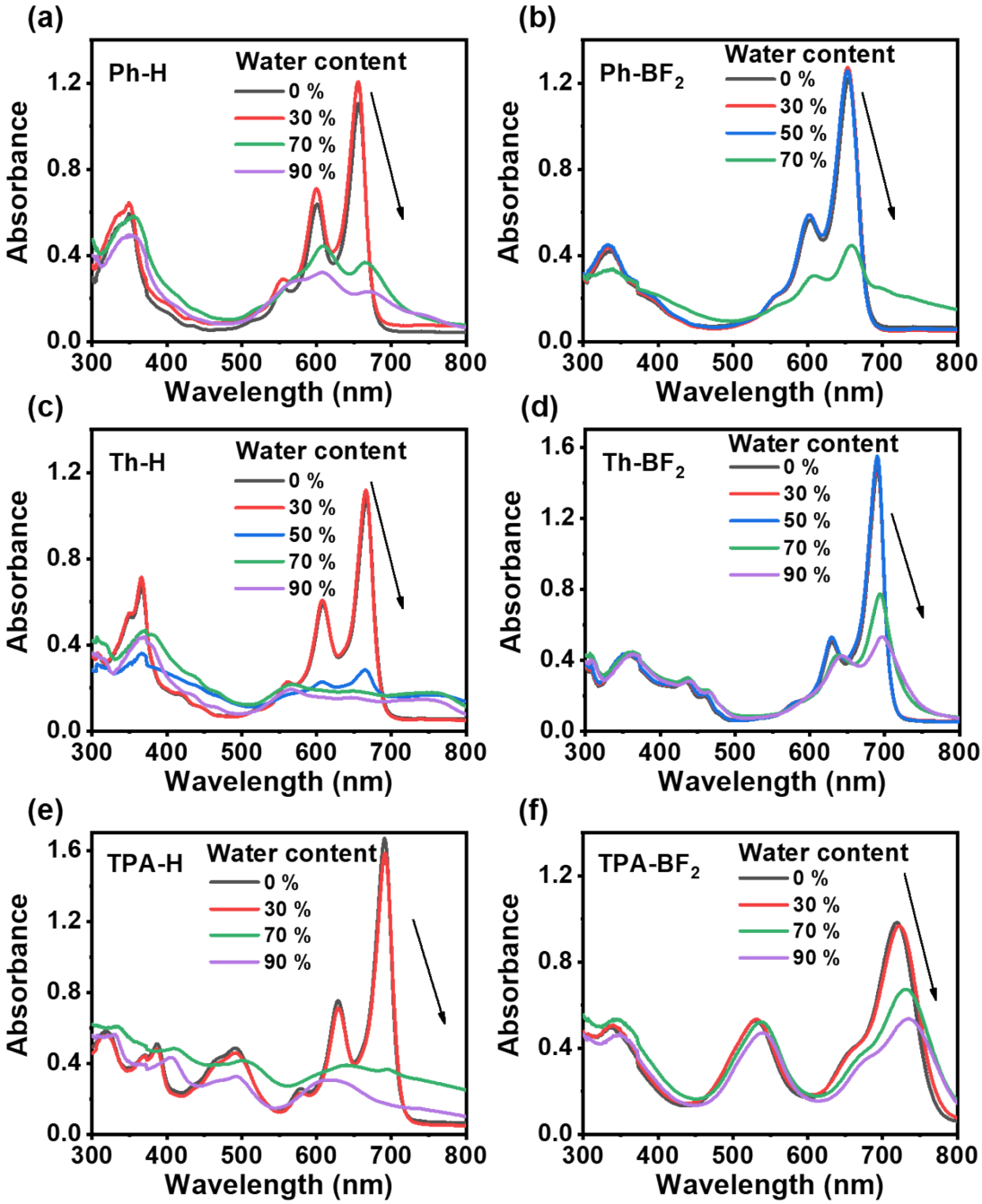

Figure S13. Absorption spectra of (a) **Ph-H,** (b) **Ph-BF$_2$,** (c) **Th-H,** (d) **Th-BF$_2$,** (e) **TPA-H** and (f) **TPA-BF$_2$** (10 μM) in THF/water mixtures.

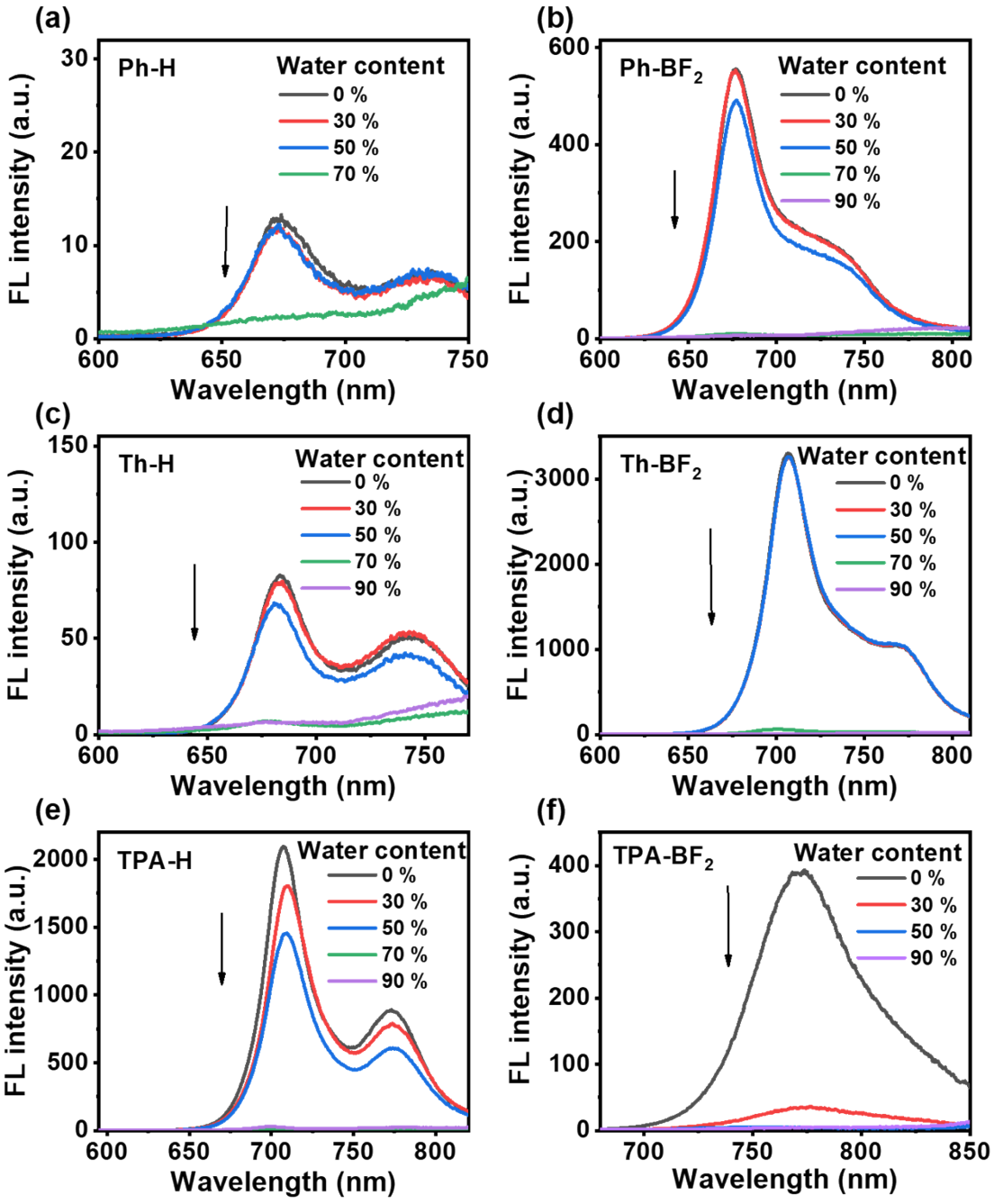

Figure S14. Emission spectra of (a) **Ph-H,** (b) **Ph-BF$_2$,** (c) **Th-H,** (d) **Th-BF$_2$,** (e) **TPA-H** and (f) **TPA-BF$_2$** (10 μM) in THF/water mixtures.

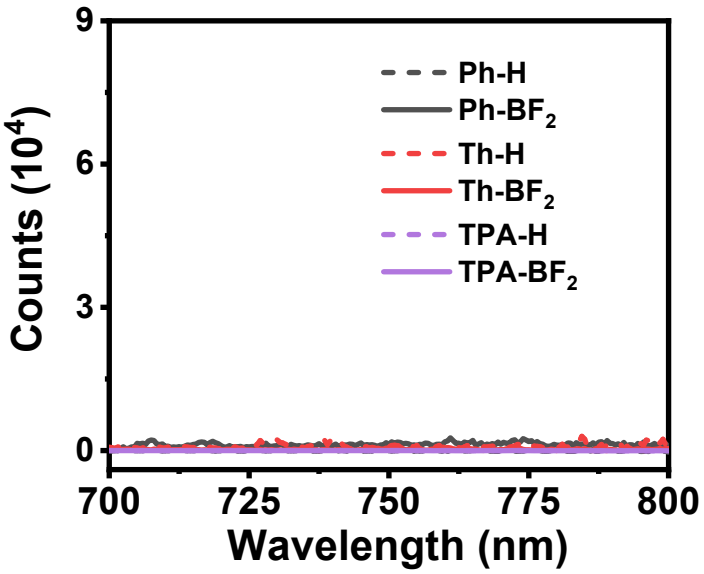

Figure S15. Emission spectra of (a) **Ph-H**, (b) **Ph-BF$_2$,** (c) **Th-H**, (d) **Th-BF$_2$**, (e) **TPA-H** and (f) **TPA-BF$_2$** powder.

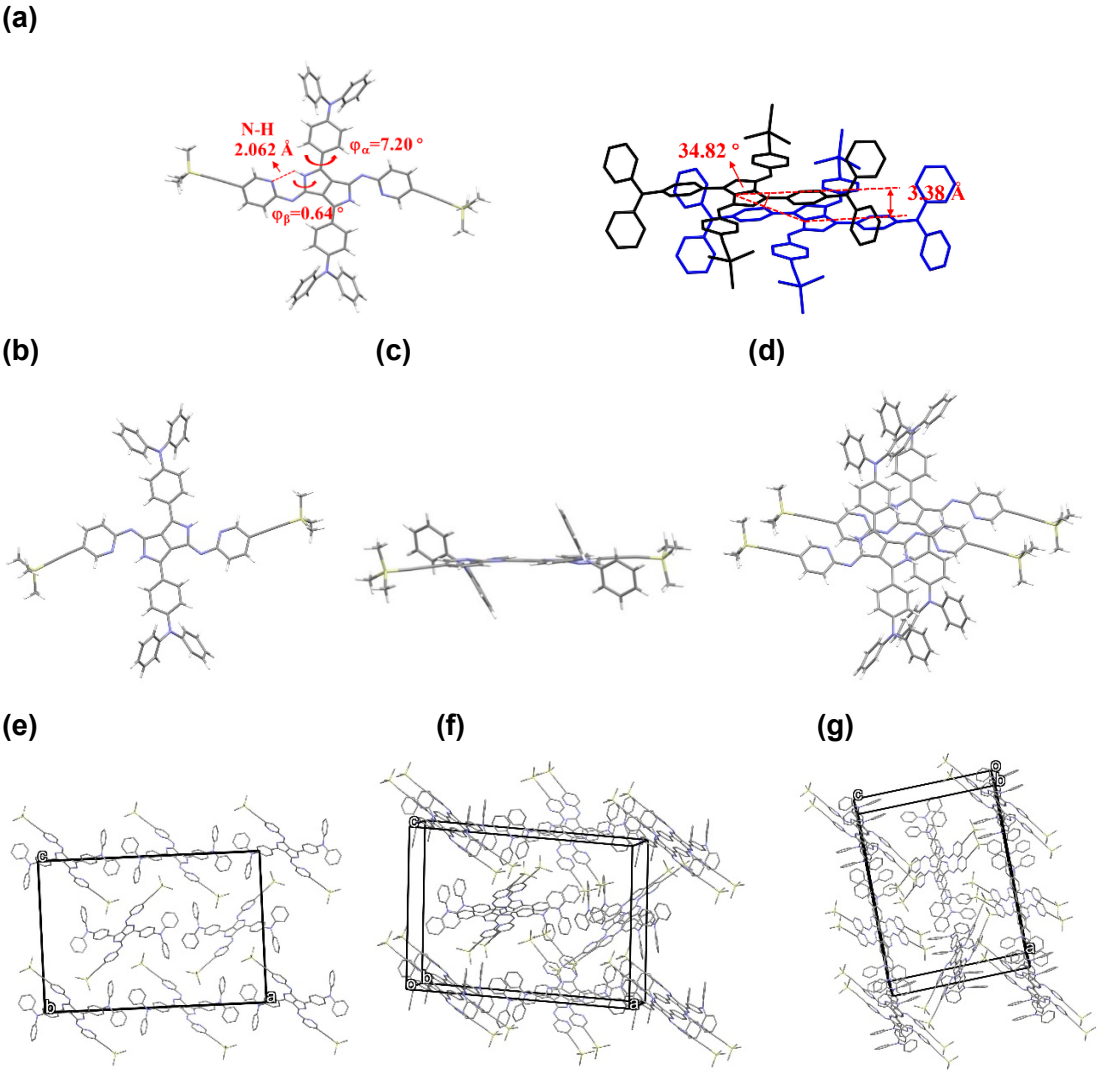

Figure S16. (a) The crystal structure of **TPA-H**. (b) The top view, (c) side view and (d) two crystal packing structure. (e-g) The solid state molecular packing graphs. Some Hydrogens are omitted for clarity.

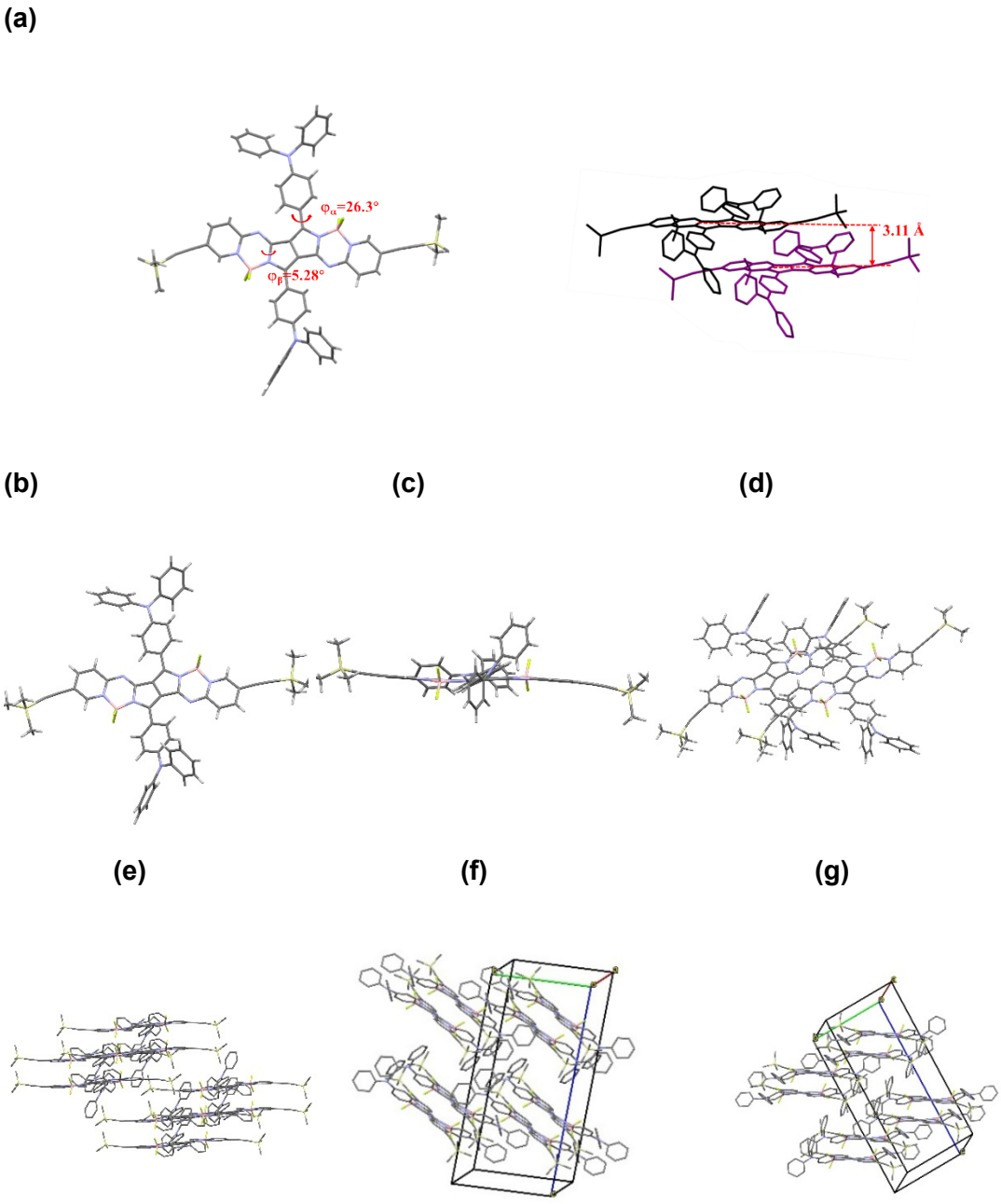

Figure S17. (a) The crystal structure of **TPA-BF$_2$**. (b) The top view, (c) side view and (d) two crystal packing structure. (e-g) The solid state molecular packing graphs. Some Hydrogens are omitted for clarity.

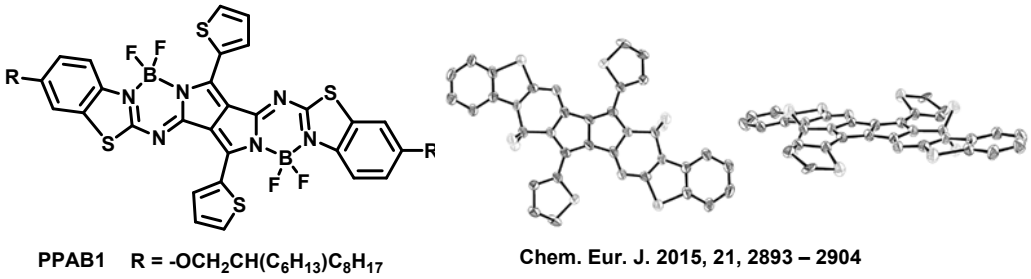

Figure S18. X-ray crystal structure of **PPAB1**, top view and side view. The thermal ellipsoids were scaled to the 50% probability level. Hydrogen atoms, 2-hexyldecyloxy substituents, and a set of the disordered thiophene rings were omitted for clarity in both views.

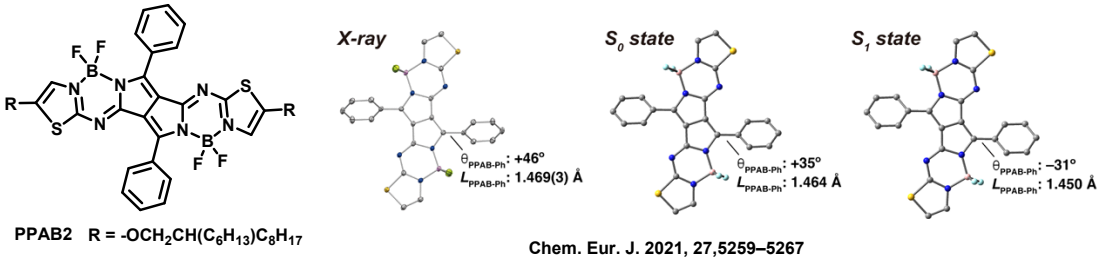

Figure S19. Structures, bond lengths, and dihedral angles of PPAB2: X-ray single crystal structure (left) and optimized structures of the S_0 (middle) and S_1 (right) states at the wB97XD/6-31G(d,p) level. θ is plus and minus for clockwise and counterclockwise rotation, respectively, when viewing from the PPAB moiety to the phenyl substituent.

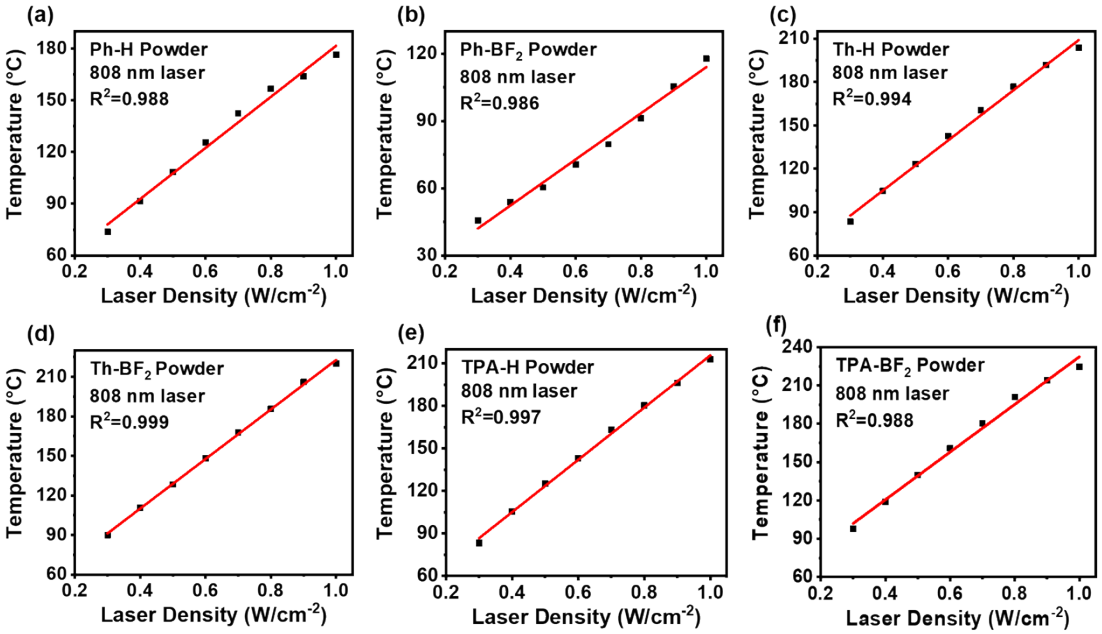

Figure S20. The fitting curve of maximum temperature and power density of (a) **Ph-H**, (b) **Ph-BF$_2$**, (c) **Th-H**, (d) **Th-BF$_2$**, (e) **TPA-H** and (f) **TPA-BF$_2$** powder.

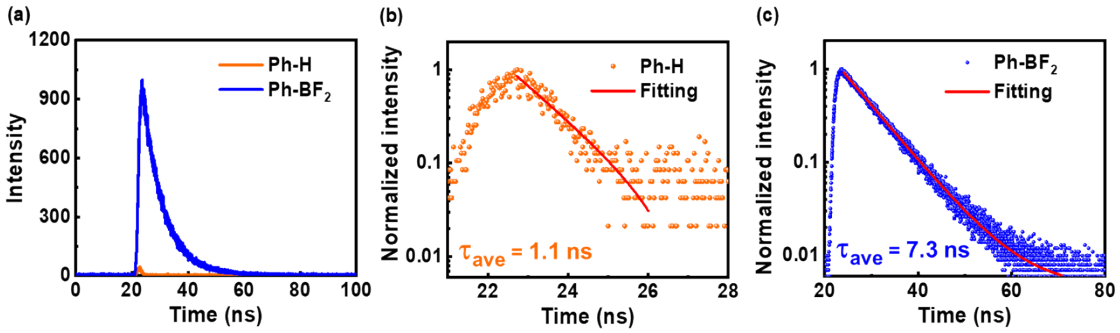

Figure S21. (a) PL decay profiles of **Ph-H** and **Ph-BF$_2$** in chloroform with excitation at 307 nm and normalized intensity of (b) **Ph-H** and (c) **Ph-BF$_2$**.

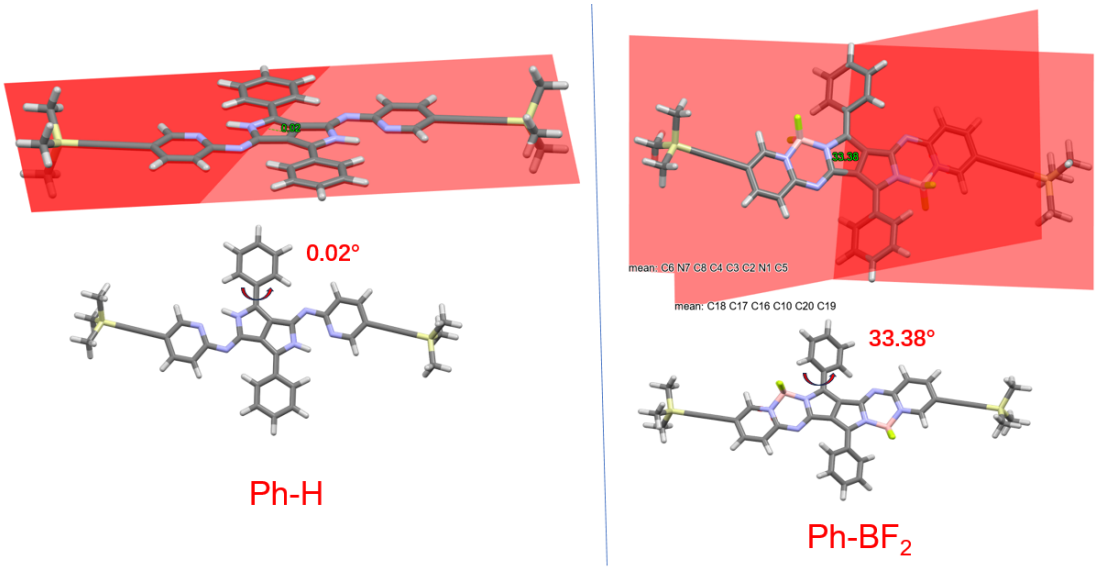

Figure S22. The dihedral angle between the side phenyl ring and the planar plane in **Ph-H** and **Ph-BF$_2$** by DFT.

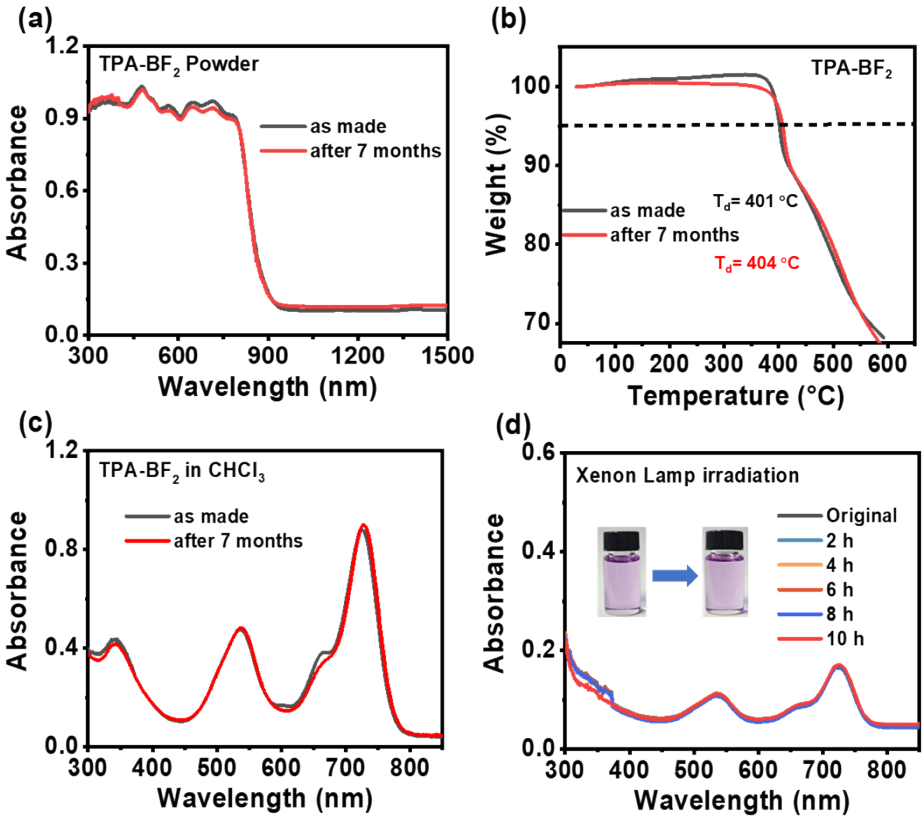

Figure S23. (a) UV-vis-NIR absorption spectra of **TPA-BF$_2$** solid. (b) TGA curves of **TPA-BF$_2$** solid. (c) The UV-Vis absorption spectra of **TPA-BF$_2$** in chloroform (10

μM). (d) The change in the UV-Vis absorption spectra of **TPA-BF$_2$** in toluene under Xe lamp irradiation (1 sun). Insets show there almost no change in **TPA-BF$_2$** solution.

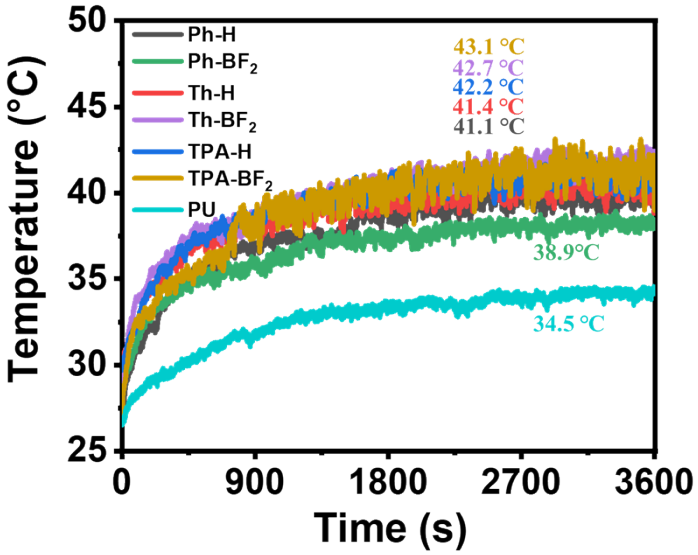

Figure S24. The heating up of the **Ph-H**, **Ph-BF$_2$**, **Th-H**, **Th-BF$_2$**, **TPA-H** and **TPA-BF$_2$**-loaded PU foams, respectively, during the evaporation of water.

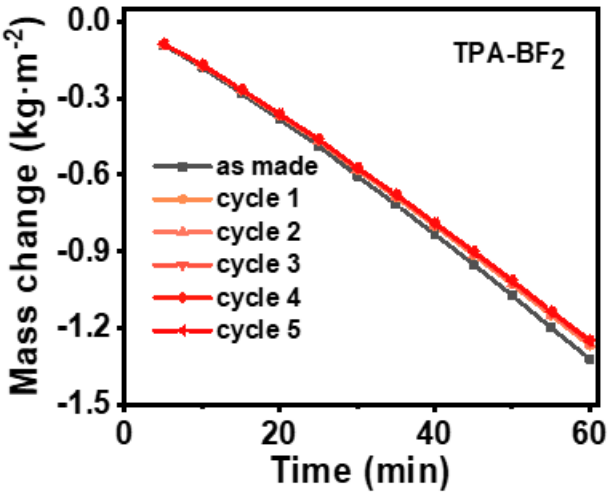

Figure S25. Mass loss curves for seawater evaporation process of **TPA-BF$_2$**-loaded PU foam (before and after storage for 7 months) within 1 h under simulated solar irradiation of 1 kW m^{-2}.

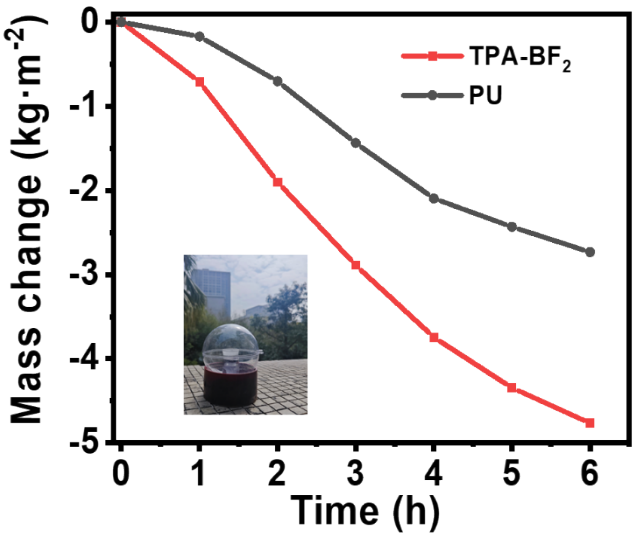

Figure S26. Time-dependent mass change of water evaporation during the test day with **TPA-BF_2**-loaded PU and pure PU as control. The inset is the photograph of the **TPA-BF_2**-loaded PU in a homemade device during daily evaporation.

Table S1. Crystal data and structure refinement for **TPA-H.**

Empirical formula	$C_{62}H_{54}N_8Si_2$
Formula weight	967.31
Temperature/K	150.00(10)
Crystal system	orthorhombic
Space group	$Pca2_1$
a/Å	35.5088(4)
b/Å	6.14840(10)
c/Å	24.3111(3)
α/°	90
β/°	90
γ/°	90
Volume/Å^3	5307.65(12)
Z	4
ρ_{calc}g/cm^3	1.211
μ/mm^{-1}	0.975
F(000)	2040.0
Crystal size/mm^3	0.13 × 0.12 × 0.1
Radiation	Cu Kα (λ = 1.54184)
2Θ range for data collection/°	4.978 to 153.122
Index ranges	-44 ≤ h ≤ 38, -7 ≤ k ≤ 6, -30 ≤ l ≤ 29
Reflections collected	28198
Independent reflections	9294 [R_{int} = 0.0288, R_{sigma} = 0.0316]
Data/restraints/parameters	9294/1/656
Goodness-of-fit on F^2	1.058
Final R indexes [I>=2σ (I)]	R_1 = 0.0372, wR_2 = 0.0989
Final R indexes [all data]	R_1 = 0.0402, wR_2 = 0.1011
Largest diff. peak/hole / e Å^{-3}	0.41/-0.24
Flack parameter	0.41(3)

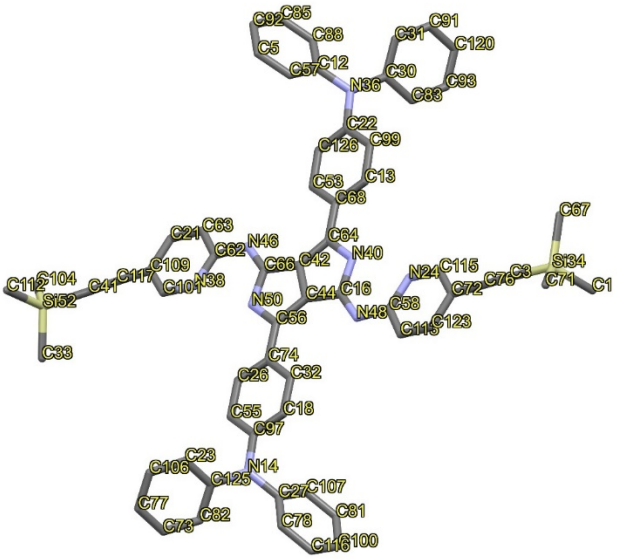

Table S2. Bond Lengths for **TPA-H.**

Atom	Atom	Length/Å	Atom	Atom	Length/Å
Si34	C3	1.852(3)	C22	C126	1.396(4)
Si34	C71	1.864(4)	C22	C99	1.392(4)
Si34	C67	1.862(3)	C26	C74	1.403(4)
Si34	C1	1.857(4)	C26	C55	1.382(4)
Si52	C41	1.843(3)	C30	C31	1.401(4)
Si52	C112	1.860(4)	C30	C83	1.393(4)
Si52	C104	1.852(3)	C32	C74	1.405(4)
Si52	C33	1.859(4)	C72	C76	1.454(4)
N46	C66	1.317(3)	C72	C115	1.386(4)
N46	C62	1.379(3)	C72	C123	1.405(4)
N50	C66	1.385(3)	C76	C3	1.181(4)
N50	C56	1.391(3)	C63	C21	1.372(4)
N36	C12	1.419(4)	C31	C91	1.379(4)
N36	C22	1.424(3)	C113	C123	1.376(4)
N36	C30	1.416(4)	C117	C109	1.445(4)
N40	C64	1.394(3)	C117	C41	1.193(4)
N40	C16	1.386(3)	C57	C5	1.382(5)
N48	C58	1.382(3)	C125	C23	1.398(4)
N48	C16	1.315(3)	C125	C82	1.397(4)
N38	C62	1.356(4)	C126	C53	1.379(4)
N38	C101	1.332(4)	C13	C99	1.386(4)
N24	C58	1.352(3)	C97	C55	1.398(4)
N24	C115	1.344(4)	C101	C109	1.395(4)

N14	C125	1.418(4)	C109	C21	1.396(4)
N14	C97	1.421(3)	C107	C27	1.389(4)
N14	C27	1.423(4)	C107	C81	1.384(5)
C42	C66	1.442(4)	C27	C78	1.396(4)
C42	C64	1.384(4)	C83	C93	1.387(5)
C42	C44	1.435(3)	C23	C106	1.379(5)
C56	C44	1.396(4)	C85	C88	1.392(5)
C56	C74	1.446(4)	C85	C92	1.377(6)
C62	C63	1.406(4)	C5	C92	1.385(5)
C68	C64	1.450(4)	C81	C100	1.383(5)
C68	C13	1.403(4)	C93	C120	1.387(5)
C68	C53	1.402(4)	C91	C120	1.377(6)
C58	C113	1.405(4)	C78	C116	1.388(5)
C44	C16	1.438(4)	C82	C73	1.389(5)
C12	C57	1.393(4)	C116	C100	1.375(6)
C12	C88	1.393(4)	C106	C77	1.395(6)
C18	C32	1.379(4)	C73	C77	1.370(6)
C18	C97	1.395(4)			

Table S3. Bond Angles for **TPA-H.**

Atom	**Atom**	**Atom**	**Angle/°**	**Atom**	**Atom**	**Atom**	**Angle/°**
C3	Si34	C71	108.86(15)	C55	C26	C74	121.5(3)
C3	Si34	C67	108.91(15)	C31	C30	N36	121.3(3)
C3	Si34	C1	107.46(15)	C83	C30	N36	120.3(2)
C67	Si34	C71	110.32(18)	C83	C30	C31	118.4(3)
C1	Si34	C71	110.5(2)	C18	C32	C74	120.5(2)
C1	Si34	C67	110.69(17)	C115	C72	C76	121.5(2)
C41	Si52	C112	106.90(16)	C115	C72	C123	117.3(2)
C41	Si52	C104	107.75(16)	C123	C72	C76	121.2(2)
C41	Si52	C33	109.38(17)	C26	C74	C56	120.6(2)
C104	Si52	C112	111.14(19)	C26	C74	C32	118.1(2)
C104	Si52	C33	111.02(18)	C32	C74	C56	121.2(2)
C33	Si52	C112	110.51(19)	C3	C76	C72	179.3(3)
C66	N46	C62	121.9(2)	N24	C115	C72	124.2(2)
C66	N50	C56	113.1(2)	C21	C63	C62	119.9(3)
C12	N36	C22	117.8(2)	C91	C31	C30	120.1(3)
C30	N36	C12	122.6(2)	C123	C113	C58	120.0(2)
C30	N36	C22	119.5(2)	C41	C117	C109	176.2(3)
C16	N40	C64	112.9(2)	C5	C57	C12	120.7(3)

C16	N48	C58	122.3(2)	C113	C123	C72	119.2(2)
C101	N38	C62	118.5(2)	C23	C125	N14	119.8(3)
C115	N24	C58	118.1(2)	C82	C125	N14	121.2(3)
C125	N14	C97	119.1(2)	C82	C125	C23	119.0(3)
C125	N14	C27	122.1(2)	C53	C126	C22	121.2(2)
C97	N14	C27	118.3(2)	C99	C13	C68	120.9(3)
C64	C42	C66	143.7(2)	C18	C97	N14	120.0(2)
C64	C42	C44	108.6(2)	C18	C97	C55	119.3(2)
C44	C42	C66	107.7(2)	C55	C97	N14	120.7(2)
N46	C66	N50	126.8(2)	N38	C101	C109	124.2(3)
N46	C66	C42	128.6(2)	C13	C99	C22	120.1(2)
N50	C66	C42	104.6(2)	C76	C3	Si34	177.1(3)
N50	C56	C44	106.2(2)	C126	C53	C68	120.1(2)
N50	C56	C74	120.7(2)	C101	C109	C117	119.5(3)
C44	C56	C74	133.1(2)	C101	C109	C21	117.0(3)
N46	C62	C63	116.6(2)	C21	C109	C117	123.5(3)
N38	C62	N46	122.7(2)	C26	C55	C97	119.7(2)
N38	C62	C63	120.7(2)	C81	C107	C27	120.5(3)
C13	C68	C64	121.4(2)	C107	C27	N14	120.4(3)
C53	C68	C64	120.0(2)	C107	C27	C78	119.4(3)
C53	C68	C13	118.6(2)	C78	C27	N14	120.2(3)
N48	C58	C113	116.0(2)	C93	C83	C30	120.7(3)
N24	C58	N48	122.9(2)	C106	C23	C125	120.5(3)
N24	C58	C113	121.1(2)	C63	C21	C109	119.7(3)
N40	C64	C68	121.3(2)	C92	C85	C88	120.7(3)
C42	C64	N40	106.2(2)	C57	C5	C92	120.0(3)
C42	C64	C68	132.4(2)	C100	C81	C107	119.9(3)
C42	C44	C16	107.8(2)	C83	C93	C120	120.4(3)
C56	C44	C42	108.4(2)	C117	C41	Si52	174.9(3)
C56	C44	C16	143.8(2)	C120	C91	C31	121.4(3)
C57	C12	N36	119.4(3)	C116	C78	C27	119.4(3)
C88	C12	N36	121.5(3)	C85	C88	C12	119.7(3)
C88	C12	C57	119.1(3)	C85	C92	C5	119.8(3)
N40	C16	C44	104.5(2)	C73	C82	C125	119.6(3)
N48	C16	N40	127.5(2)	C100	C116	C78	120.9(3)
N48	C16	C44	128.0(2)	C116	C100	C81	119.9(3)
C32	C18	C97	120.9(3)	C91	C120	C93	118.9(3)
C126	C22	N36	120.2(2)	C23	C106	C77	120.2(4)
C99	C22	N36	120.8(2)	C77	C73	C82	121.2(3)
C99	C22	C126	119.0(2)	C73	C77	C106	119.4(3)

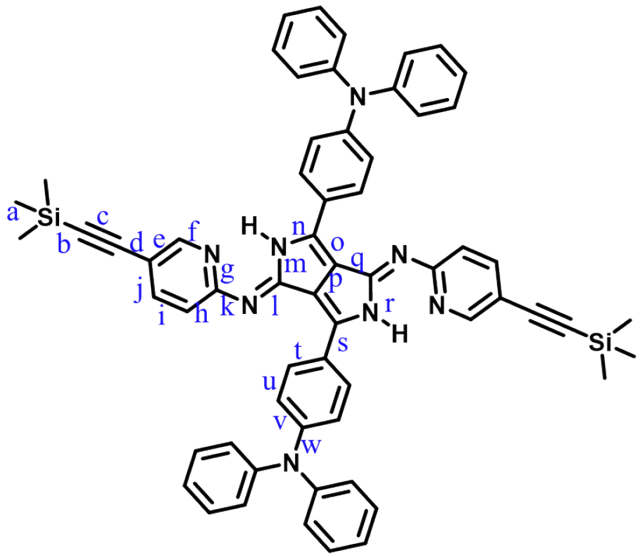

Table S4. Comparison of **TPA-H** from DFT calculations and X-ray single-crystal.

	DFT	XRD	Δ		DFT	Single crystal	Δ
a	1.886	1.859	0.027	m	1.394	1.385	0.009
b	1.833	1.843	-0.01	n	1.387	1.391	-0.004
c	1.221	1.193	0.028	o	1.395	1.397	-0.002
d	1.419	1.445	-0.026	p	1.439	1.435	0.004
e	1.404	1.395	0.009	q	1.441	1.438	0.003
f	1.331	1.332	-0.001	r	1.018	0.880	0.138
g	1.362	1.357	0.005	s	1.444	1.450	-0.006
h	1.416	1.405	0.011	t	1.411	1.402	0.009
i	1.378	1.373	0.005	u	1.384	1.379	0.005
j	1.414	1.396	0.018	v	1.407	1.396	0.011
k	1.371	1.379	-0.008	w	1.405	1.423	-0.018
l	1.312	1.318	-0.006				

Table S5. Crystal data and structure refinement for **TPA-BF_2.**

Empirical formula	$C_{62}H_{52}B_2F_4N_8Si_2$
Formula weight	1062.91
Temperature/K	100.4(9)
Crystal system	triclinic
Space group	P-1
a/Å	8.0962(3)
b/Å	13.0952(4)
c/Å	28.1636(8)
α/°	78.261(3)
β/°	83.438(3)
γ/°	85.989(3)
Volume/Å3	2900.99(17)
Z	2
ρcalcg/cm3	1.217
μ/mm-1	1.035
F(000)	1108.0
Crystal size/mm3	0.15 × 0.13 × 0.11
Radiation	Cu Kα (λ = 1.54184)
2Θ range for data collection/°	6.444 to 150.54
Index ranges	$-10 \leq h \leq 10$, $-12 \leq k \leq 15$, $-34 \leq l \leq 35$
Reflections collected	31627
Independent reflections	11064 [R_{int} = 0.0456, R_{sigma} = 0.0338]
Data/restraints/parameters	11064/0/709
Goodness-of-fit on F2	1.052
Final R indexes [I>=2σ (I)]	R1 = 0.0887, wR2 = 0.2214
Final R indexes [all data]	R1 = 0.0958, wR2 = 0.2253
Largest diff. peak/hole / e Å-3	0.56/-0.51

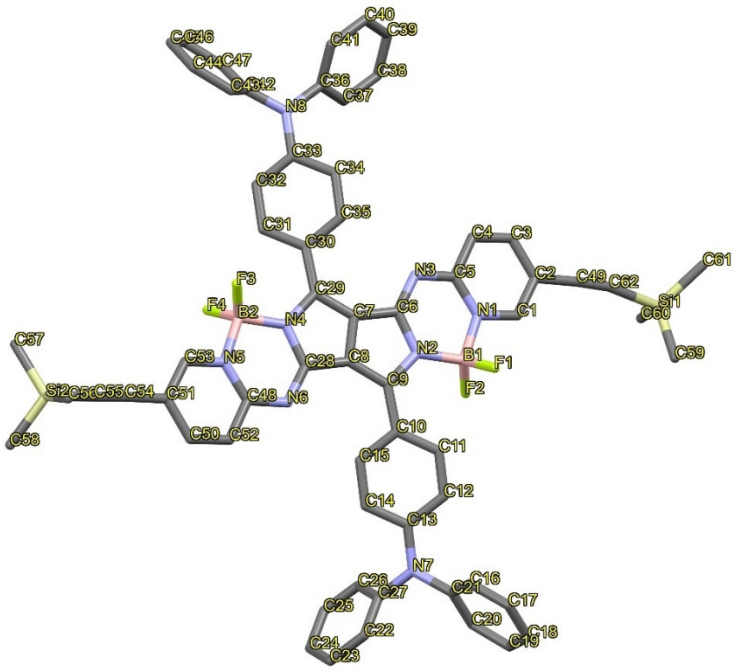

Table S6. Bond Lengths for **TPA-BF$_2$.**

Atom	Atom	Length/Å	Atom	Atom	Length/Å
Si1	C59	1.853(8)	C10	C11	1.404(5)
Si1	C60	1.855(5)	C10	C15	1.416(5)
Si1	C61	1.843(7)	C11	C12	1.373(5)
Si1	C62	1.872(5)	C12	C13	1.402(5)
Si2	C55	1.881(5)	C13	C14	1.393(5)
Si2	C56	1.857(6)	C14	C15	1.377(5)
Si2	C57	1.838(7)	C16	C17	1.384(6)
Si2	C58	1.864(5)	C16	C21	1.391(6)
F1	B1	1.396(5)	C17	C18	1.388(6)
F2	B1	1.369(5)	C18	C19	1.381(7)
F3	B2	1.375(5)	C19	C20	1.388(6)
F4	B2	1.389(5)	C20	C21	1.390(6)
N1	C1	1.371(5)	C22	C23	1.400(6)
N1	C5	1.363(5)	C22	C27	1.384(6)
N1	B1	1.584(5)	C23	C24	1.375(7)
N2	C6	1.391(5)	C24	C25	1.377(7)
N2	C9	1.410(4)	C25	C26	1.392(6)
N2	B1	1.534(5)	C26	C27	1.389(6)
N3	C5	1.352(5)	C29	C30	1.452(5)

N3	C6	1.321(5)	C30	C31	1.402(5)
N4	C28	1.393(5)	C30	C35	1.400(5)
N4	C29	1.410(4)	C31	C32	1.378(5)
N4	B2	1.538(5)	C32	C33	1.400(6)
N5	C48	1.358(5)	C33	C34	1.409(5)
N5	C53	1.358(5)	C34	C35	1.374(5)
N5	B2	1.587(5)	C36	C37	1.382(6)
N6	C28	1.315(5)	C36	C41	1.387(6)
N6	C48	1.357(5)	C37	C38	1.386(6)
N7	C13	1.406(5)	C38	C39	1.382(6)
N7	C21	1.422(5)	C39	C40	1.371(6)
N7	C27	1.438(5)	C40	C41	1.392(6)
N8	C33	1.402(5)	C42	C43	1.384(7)
N8	C36	1.425(5)	C42	C47	1.399(6)
N8	C42	1.428(5)	C43	C44	1.384(7)
C1	C2	1.371(5)	C44	C45	1.384(8)
C2	C3	1.410(6)	C45	C46	1.376(8)
C2	C49	1.457(5)	C46	C47	1.387(6)
C3	C4	1.359(5)	C48	C52	1.413(5)
C4	C5	1.425(5)	C49	C62	1.147(6)
C6	C7	1.443(5)	C50	C51	1.417(6)
C7	C8	1.415(5)	C50	C52	1.366(5)
C7	C29	1.391(5)	C51	C53	1.372(5)
C8	C9	1.406(5)	C51	C54	1.474(6)
C8	C28	1.435(5)	C54	C55	1.128(6)
C9	C10	1.454(5)			

Table S7. Bond Angles for **TPA-BF_2.**

Atom	**Atom**	**Atom**	**Angle/°**	**Atom**	**Atom**	**Atom**	**Angle/°**
C59	Si1	C60	111.1(3)	C16	C21	N7	121.0(4)
C59	Si1	C62	103.7(3)	C20	C21	N7	120.1(4)
C60	Si1	C62	108.3(2)	C20	C21	C16	118.9(4)
C61	Si1	C59	112.9(5)	C27	C22	C23	119.7(4)
C61	Si1	C60	108.6(3)	C24	C23	C22	120.4(4)
C61	Si1	C62	112.1(3)	C23	C24	C25	119.9(4)
C56	Si2	C55	108.2(2)	C24	C25	C26	120.2(5)
C56	Si2	C58	109.9(3)	C27	C26	C25	120.1(4)
C57	Si2	C55	108.1(3)	C22	C27	N7	119.6(4)
C57	Si2	C56	110.7(4)	C22	C27	C26	119.6(4)

C57	Si2	C58	110.6(3)	C26	C27	N7	120.8(4)
C58	Si2	C55	109.4(2)	N4	C28	C8	106.9(3)
C1	N1	B1	116.3(3)	N6	C28	N4	126.0(3)
C5	N1	C1	120.1(3)	N6	C28	C8	127.1(3)
C5	N1	B1	123.4(3)	N4	C29	C30	125.1(3)
C6	N2	C9	109.8(3)	C7	C29	N4	106.6(3)
C6	N2	B1	120.9(3)	C7	C29	C30	128.3(3)
C9	N2	B1	129.2(3)	C31	C30	C29	124.6(3)
C6	N3	C5	119.6(3)	C35	C30	C29	117.8(3)
C28	N4	C29	110.1(3)	C35	C30	C31	117.5(3)
C28	N4	B2	121.1(3)	C32	C31	C30	121.6(4)
C29	N4	B2	128.8(3)	C31	C32	C33	120.4(4)
C48	N5	C53	120.4(3)	N8	C33	C34	121.0(3)
C48	N5	B2	123.2(3)	C32	C33	N8	120.4(4)
C53	N5	B2	116.2(3)	C32	C33	C34	118.5(3)
C28	N6	C48	119.5(3)	C35	C34	C33	120.3(3)
C13	N7	C21	122.2(3)	C34	C35	C30	121.7(4)
C13	N7	C27	120.0(3)	C37	C36	N8	120.5(4)
C21	N7	C27	117.8(3)	C37	C36	C41	119.9(4)
C33	N8	C36	120.7(3)	C41	C36	N8	119.5(4)
C33	N8	C42	120.6(3)	C36	C37	C38	119.9(4)
C36	N8	C42	118.5(3)	C39	C38	C37	120.2(4)
N1	C1	C2	122.4(4)	C40	C39	C38	119.9(4)
C1	C2	C3	118.0(3)	C39	C40	C41	120.4(4)
C1	C2	C49	118.8(4)	C36	C41	C40	119.6(4)
C3	C2	C49	123.3(3)	C43	C42	N8	120.4(4)
C4	C3	C2	120.2(4)	C43	C42	C47	119.6(4)
C3	C4	C5	120.4(4)	C47	C42	N8	120.0(4)
N1	C5	C4	118.8(3)	C42	C43	C44	120.0(5)
N3	C5	N1	122.3(3)	C45	C44	C43	120.1(5)
N3	C5	C4	118.8(3)	C46	C45	C44	120.4(4)
N2	C6	C7	107.5(3)	C45	C46	C47	119.8(4)
N3	C6	N2	126.0(3)	C46	C47	C42	120.0(5)
N3	C6	C7	126.5(3)	N5	C48	C52	119.0(3)
C8	C7	C6	106.4(3)	N6	C48	N5	122.7(3)
C29	C7	C6	143.8(3)	N6	C48	C52	118.3(3)
C29	C7	C8	109.7(3)	C62	C49	C2	176.4(5)
C7	C8	C28	106.7(3)	C52	C50	C51	120.0(4)
C9	C8	C7	109.5(3)	C50	C51	C54	121.0(3)
C9	C8	C28	143.8(3)	C53	C51	C50	117.4(3)

N2	C9	C10	123.9(3)	C53	C51	C54	121.6(4)
C8	C9	N2	106.8(3)	C50	C52	C48	120.4(4)
C8	C9	C10	129.2(3)	N5	C53	C51	122.8(4)
C11	C10	C9	125.8(3)	C55	C54	C51	175.7(5)
C11	C10	C15	116.9(3)	C54	C55	Si2	175.3(5)
C15	C10	C9	117.3(3)	C49	C62	Si1	169.0(4)
C12	C11	C10	121.2(3)	F1	B1	N1	106.1(3)
C11	C12	C13	121.5(3)	F1	B1	N2	111.8(3)
C12	C13	N7	121.5(3)	F2	B1	F1	110.2(3)
C14	C13	N7	120.9(3)	F2	B1	N1	108.4(3)
C14	C13	C12	117.6(3)	F2	B1	N2	113.1(3)
C15	C14	C13	121.3(4)	N2	B1	N1	106.9(3)
C14	C15	C10	121.2(3)	F3	B2	F4	110.1(3)
C17	C16	C21	120.3(4)	F3	B2	N4	112.5(3)
C16	C17	C18	121.0(4)	F3	B2	N5	108.8(3)
C19	C18	C17	118.6(4)	F4	B2	N4	112.9(3)
C18	C19	C20	121.0(4)	F4	B2	N5	105.4(3)
C19	C20	C21	120.2(4)	N4	B2	N5	106.7(3)

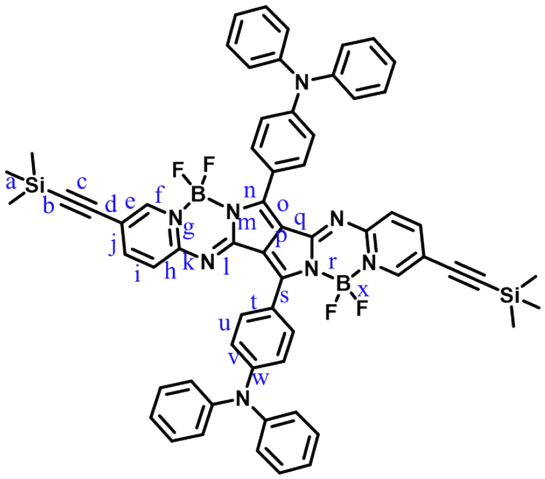

Table S8. Comparison of **TPA-BF$_2$** from DFT calculations and X-ray single-crystal.

	DFT	XRD	Δ		DFT	Single crystal	Δ
a	1.885	1.839	0.046	m	1.398	1.393	0.005
b	1.838	1.881	-0.043	n	1.398	1.410	-0.012
c	1.220	1.128	0.092	o	1.400	1.391	0.009
d	1.420	1.474	-0.054	p	1.426	1.414	0.012
e	1.386	1.372	0.014	q	1.427	1.443	-0.016
f	1.351	1.358	-0.007	r	1.543	1.533	0.010
g	1.373	1.359	0.014	s	1.451	1.454	-0.003
h	1.420	1.412	0.008	t	1.411	1.416	-0.005
i	1.370	1.365	0.005	u	1.383	1.377	0.006
j	1.424	1.418	0.006	v	1.407	1.393	0.014
k	1.343	1.357	-0.014	w	1.404	1.405	-0.001
l	1.324	1.315	0.009	x	1.380	1.369	0.011

Table S9. The summary of the previously reported materials for water evaporation in recent years.

Compound	T_{max} (°C) [a]	T_d [b] (°C)	Solid / Solution absorption range	Voltage (mV)	Water evaporation	Ref
TPyP	~140 (730 nm laser 0.8 W cm^{-2})	480	300-800 nm (solid)-	60	56.0%	1
DDPA-PDN	201 (655 nm laser 0.9 W cm^{-2})	447	300-850 nm (solid)	83	73.98%	2
TMBZ-TCNB	68.4 (808 nm laser 0.6 W cm^{-2})	220	220-1100 nm （solid）	-	63.49%	3
TPP-2IND	~190 (660 nm laser 0.9 W cm^{-2})	300	300-600 (solution)	-	65.8%	4
DPP-INCN	-	-	350-900 nm (solution)	-	70.2%	5
BQC	55 (1 Sun)	310	300-1000 nm (solid)-	97.0	72%	6
BQE	65 (1 Sun)	418	300-1000 nm (solid)	112.8	83%	6
T-TTD-T	~122 (685 nm laser 0.6 W cm^{-2})	200	300-1000 nm (solid)	-	85.2%	7
4OCSPC	69.5 (Solar source 200 mW cm^{-2})	289	300-1000 nm (solid)	221	86.6%	8
CR-TPE-T	~110 (808 nm laser 1.0 W cm^{-2})	-	300-1600 nm (solid)	-	87.2%	9
CR-$(DPA)_2$-OMe	130 (808 nm laser 0.5 W cm^{-2})	340	300-2500 nm (solid)	-	92.6%	10
P3HT	~50 (1 Sun)	-	300-900 nm (solid)	124	86.0%	11
DDHT	227 (655 nm laser 0.8 W cm^{-2})	328	300-950 nm (solid)	179.5	78.4%	12

DCN-4CQA	57 (Solar source 200 mW cm^{-2})	335	300-800 nm (solid)	224	66.84%	13
Ph-H	176.5 (808 nm laser 1.0 W cm^{-2})	360	300-1000 nm (solid)	162	76.4%	This work
Ph-BF_2	117.9 (808 nm laser 1.0 W cm^{-2})	384	300-900 nm (solid)	137	62.9%	This work
Th-H	203.7 (808 nm laser 1.0 W cm^{-2})	360	300-1000 nm (solid)	180	77.5%	This work
Th-BF_2	220.1 (808 nm laser 1.0 W cm^{-2})	389	300-1000 nm (solid)	192	84.9%	This work
TPA-H	213.1 (808 nm laser 1.0 W cm^{-2})	417	300-1000 nm (solid)	187	83.7%	This work
TPA-BF_2	224.5 (808 nm laser 1.0 W cm^{-2})	401	300-1000 nm (solid)	198	90.5%	This work

[b] The highest temperature of photothermal material under simulated sunlight. [b] the temperature at which 5 % weight loss.

Table s10. Environmental parameters of outdoor test

Mass change of water in TPA-BF_2 system (g)	Mass change of water in PU system (g)	Time	Surrounding temperature (°C)	Humidity (%)	UV Index	Atm. pressure (hpa)	Weather
0	0	12:00	23.5	71	8	1010	cloudy
-0.223	-0.054	13:00	29.8	41	8	1009	sunny
-0.597	-0.221	14:00	32.0	35	8	1008	sunny
-0.907	-0.451	15:00	29.6	39	6	1007	sunny
-1.176	-0.658	16:00	27.1	44	4	1006	cloudy
-1.364	-0.764	17:00	26.9	44	2	1006	cloudy
-1.496	-0.858	18:00	25.6	49	1	1006	cloudy

References

1. Y. Zhang, H. Yan, X. Wang, Z. Zhang, F. Liu, S. Tu and X. Chen, Highly efficient solar-absorber composite material based on tetrapyridylporphyrin for water evaporation and thermoelectric power generation, *RSC Advances*, 2022, **12**, 28997-29002.
2. Y. Cui, J. Liu, Z. Li, M. Ji, M. Zhao, M. Shen, X. Han, T. Jia, C. Li and Y. Wang, Donor–Acceptor-Type Organic-Small-Molecule-Based Solar-Energy-Absorbing Material for Highly Efficient Water Evaporation and Thermoelectric Power Generation, *Advanced Functional Materials*, 2021, **31**, 2106247.
3. M. Jiang, Y. Su, S. Li, S. Fu, L. Wang, D. Khan, Y. Sun, L. Sun, X. Zhang and W. Hu, Organic photothermal cocrystal with high stability for efficient solar-driven water evaporation, *Journal of Materials Chemistry C*, 2023, **11**, 13274-13280.
4. J.-C. Yang, L. Wu, L. Wang, R. Ren, P. Chen, C. Qi, H.-T. Feng and B. Z. Tang, An efficient photothermal conversion material based on D-A type luminophore for solar-driven desalination, *Aggregate*, 2024, **5**, e535.
5. S. P. Prakoso, S.-S. Sun, R. Saleh, Y.-T. Tao and C.-L. Wang, Tailoring Photophysical Properties of Diketopyrrolopyrrole Small Molecules with Electron-Withdrawing Moieties for Efficient Solar Steam Generation, *ACS Applied Materials & Interfaces*, 2021, **13**, 38365-38374.
6. J. Li, L. Wang, C. Zhang, H. Wang, Y. Pan, S. Li, X.-K. Chen, T. Jia and K. Wang, Manipulation of the Self-Assembly Morphology by Side-Chain Engineering of Quinoxaline-Substituted Organic Photothermal Molecules for Highly Efficient Solar-Thermal Conversion and Applications, *Angewandte Chemie International Edition*, 2024, **63**, e202402726.
7. L. Guo, X. Kong, R. Li, J. Sun, G. Wang and X. Gu, Low-molecular-weight organic small-molecule photothermal material for high-efficiency solar-thermal water evaporation, *Dyes and Pigments*, 2024, **227**, 112195.
8. X. Han, Z. Wang, M. Shen, J. Liu, Y. Lei, Z. Li, T. Jia and Y. Wang, A highly efficient organic solar energy-absorbing material based on phthalocyanine derivative for integrated water evaporation and thermoelectric power generation application, *Journal of Materials Chemistry A*, 2021, **9**, 24452-24459.
9. G. Chen, J. Sun, Q. Peng, Q. Sun, G. Wang, Y. Cai, X. Gu, Z. Shuai and B. Z. Tang, Biradical-Featured Stable Organic-Small-Molecule Photothermal Materials for Highly Efficient Solar-Driven Water Evaporation, *Advanced Materials*, 2020, **32**, 1908537.
10. L. Yang, G. Wang, Y. Zhang, J. Zhou, R. Wu, C. Qin, Q. Chang, C. Zhang, S. Duan and X. Gu, Radical-Assisted Nonradiative Processes to Couple Photothermy and Photosensitization for Solar-Driven Water Evaporation, *Angewandte Chemie International Edition*, 2025, **64**, e202508821.
11. L. Wang, G. Xi, Z. Chen, Q. Wang, J. Liu, R. Zhang, T. Jia and X. Zhao, The efficient photothermal performance of organic polymeric material poly3-hexylthiophene for solar driven water evaporation and thermoelectric power generation, *Journal of Solid State Chemistry*, 2023, **324**, 124081.
12. M. Zhao, Y. Zhu, Y. Pan, Y. Wang, T. Xu, X. Zhao, T. Jia, Z. Zhang and Z. Chen, High-Performance Organic Photothermal Material Based on Fusion of the Donor–Acceptor Structure for Water Evaporation and Thermoelectric Power Generation, *ACS Applied*

Energy Materials, 2022, **5**, 15758-15767.

13. M. Shen, X. Zhao, L. Han, N. Jin, S. Liu, T. Jia, Z. Chen and X. Zhao, Developing Flexible Quinacridone-Derivatives-Based Photothermal Evaporaters for Solar Steam and Thermoelectric Power Generation, *Chemistry – A European Journal*, 2022, **28**, e202104137.
14. Y. Gan, B. Lu, J. Zhong, X. Ran, D. Cao and L. Wang, A Galactose-Functionalized Pyrrolopyrrole Aza-BODIPY for Highly Efficient Detection of Eight Aliphatic and Aromatic Biogenic Amines: Monitoring Food Freshness and Bioimaging, *Biosensors*, 2025, **15**, 542.
15. B. Lai, Y. Xiao, Y. Zhang, J. Huang, Y. Yang, J. Rui , D. Cao, X. Ran, Z. Kuang, Y. Li and L. Wang, Less is Better: Facilely Boosting Highly Efficient Pho-to-thermal-electric Conversion via Ultra-Stable Donor-acceptor Singlet Diradicals, *Science China Chemistry*, 2025, https://doi.org/10.1007/s11426-025-3084-7.